Ecoclimates: Climate-Response Modeling of Vegetation

WOJTEK PAŁUBICKI, UAM, Poland
MIŁOSZ MAKOWSKI, UAM, Poland
WERONIKA GAJDA, UAM, Poland
TORSTEN HÄDRICH, KAUST, KSA
DOMINIK L. MICHELS, KAUST, KSA
SÖREN PIRK, Adobe Research*, USA

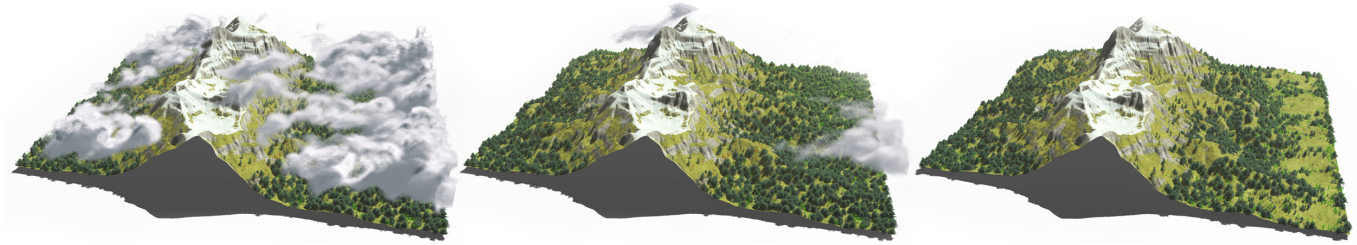

Fig. 1. We simulate ecoclimates by combining models for vegetation, soil, and weather. This allows us to simulate complex and realistic outdoor landscapes with vegetation growth and weather dynamics (left, center). Our method can simulate over 500K plants with individual geometries at interactive rates (center). Additionally, we can also simulate the climate-response of vegetation, e.g. resulting in forest dieback (right).

One of the greatest challenges to mankind is understanding the underlying principles of climate change. Over the last years, the role of forests in climate change has received increased attention. This is due to the observation that not only the atmosphere has a principal impact on vegetation growth but also that vegetation is contributing to local variations of weather resulting in diverse microclimates. The interconnection of plant ecosystems and weather is described and studied as ecoclimates. In this work we take steps towards simulating ecoclimates by modeling the feedback loops between vegetation, soil, and atmosphere. In contrast to existing methods that only describe the climate at a global scale, our model aims at simulating local variations of climate. Specifically, we model tree growth interactively in response to gradients of water, temperature and light. As a result, we are able to capture a range of ecoclimate phenomena that have not been modeled before, including geomorphic controls, forest edge effects, the Foehn effect and spatial vegetation patterning. To validate the plausibility of our method we conduct a comparative analysis to studies from ecology and climatology. Consequently, our method advances the state-of-the-art of generating highly realistic outdoor landscapes of vegetation.

CCS Concepts: • **Computing methodologies** → **Physical simulation**.

*Work done at Google Research.

Authors' addresses: Wojtek Pałubicki, wojciech.palubicki@amu.edu.pl, UAM, Umultowska 87, 61-614 Poznań, Poland; Miłosz Makowski, milosz.makowski@amu.edu.pl, UAM, Umultowska 87, 61-614 Poznań, Poland; Weronika Gajda, wersko3@st.amu.edu.pl, UAM, Umultowska 87, 61-614 Poznań, Poland; Torsten Hädrich, torsten.hadrich@kaust.edu.sa, KAUST, Visual Computing Center, Thuwal 23955, KSA; Dominik L. Michels, dominik.michels@kaust.edu.sa, KAUST, Visual Computing Center, Thuwal 23955, KSA; Sören Pirk, soeren.pirk@gmail.com, Adobe Research* , 345 Park Avenue San Jose, CA 95110-2704, USA.

0730-0301/2022/7-ART155 $15.00
https://doi.org/10.1145/3528223.3530146

Additional Key Words and Phrases: Cloud Simulation, Fluid Dynamics, Physics-based Modeling and Simulation, Weather Simulation, Vegetation Modeling, Natural Phenomena, Interactive Modeling, Plant Ecosystems.

ACM Reference Format:
Wojtek Pałubicki, Miłosz Makowski, Weronika Gajda, Torsten Hädrich, Dominik L. Michels, and Sören Pirk. 2022. Ecoclimates: Climate-Response Modeling of Vegetation. *ACM Trans. Graph.* 41, 4, Article 155 (July 2022), 19 pages. https://doi.org/10.1145/3528223.3530146

1 INTRODUCTION

Understanding the complex interconnection of plant ecosystems and their impact on the climate system plays a central role in predicting climate dynamics. While it is well understood that climatic variations cause changes in ecosystem distribution, structure and function, only recently it has been recognized that the composition of vegetation also impacts the development of weather, which – in turn – leads to the development of local climatic variation (microclimates) [Bastiaansen et al. 2020]. Researchers study the interconnection of plant ecosystems and their impact on the climate system as *ecoclimates*. Understanding these ecoclimates is a challenging and open research problem.

The primary goals of ecoclimate research are to understand the growth response and functioning of vegetation according to changing climatic conditions [Liang et al. 2019], the impact of vegetation on thermodynamics and the water cycle [Allan et al. 2020], and the feedback loop of vegetation and the climate [Kovenock and Swann 2018]. Many of the current approaches for modeling ecoclimate processes rely on meteorological or macroclimate data, such as free-air temperature or open-field precipitation, that is measured in weather stations. However, recent studies indicate that climatic parameters in forests are determined to a greater degree by microclimatic rather than macroclimatic processes [Zellweger et al. 2020]. Furthermore, most of the analytical ecoclimate approaches do not

leverage geometric representations of individual plants to explore vegetation-climate interactions but instead treat plants as averaged populations.

In computer graphics, modeling plant ecosystems has a long tradition [Deussen et al. 2002, 1998; Jaeger and Teng 2003; Lane and Prusinkiewicz 2002], that more recently also encompasses complex physical simulations, such as required for modeling wildfires [Hädrich et al. 2021], erosion feedback [Cordonnier et al. 2017], or the interaction with fauna [Ecormier-Nocca et al. 2021]. The goal of many of these methods is to employ detailed geometric representations to faithfully simulate the underlying physical or biological processes. The breadth of these approaches is a testament of the complexity of this undertaking. Simulating the growth response of vegetation according to climatic variations and the impact of vegetation on local weather and climate has not yet been studied in computer graphics. Closest to this objective is the method of Makowski et al. [2019], who simulate the development of plant ecosystems in different climatic conditions. However, their method only simulates the feedback from the atmosphere to vegetation at a global scale disregarding the influence of the microclimate.

In this paper, we propose a method to capture feedback loops between vegetation, soil, and the atmosphere at a local scale. We extend existing vegetation and atmosphere models and combine them with a novel soil model. This allows us to jointly simulate the hydrologic cycle, heat transfer, and light availability. We model tree growth interactively in response to gradients of water, temperature and light. As a result, we are able to capture a range of ecoclimate phenomena that have not been emergently modeled before, including geomorphic controls, forest edge effects, the Foehn effect and spatial vegetation patterning. This not only allows us to generate highly realistic outdoor landscapes of vegetation, but also to capture essential ecoclimate variations resulting from deforestation and drought.

Our framework allows us to interactively explore complex ecoclimate phenomena by explicitly considering climatic gradients. This is the first attempt that combines a detailed vegetation growth model with a climate representation comprised of a hydrological cycle, heat transfer, and a light model. Unlike existing methods in climatology that focus on physically detailed representations of these processes, our goal is to find a light-weight description that emergently captures ecoclimate-related phenomena. For this reason, we refrain from a detailed description of irradiance. Our approach considers the geometry of individual plants, the terrain, and cloud formation to simulate climates locally. We show that explicitly modeling 3D geometry and simulating physically and biologically plausible scenes enables studying microclimate phenomena.

To summarize, our contributions are as follows: (1) we propose a novel model for simulating ecoclimates that allows us to plausibly model vegetation-climate feedback loops for individual trees ; (2) our method is the first to simulate gradients of water, temperature and light which allows capturing local phenomena of vegetation development, such as varying vegetation distribution at forest edges, the formation of spots, stripes, and gaps, as well as complex geomorphic effects; (3) we validate the plausibility of our method through numerous experiments and by comparing our results to studies from ecology and climatology.

2 RELATED WORK

In this section, we aim to provide an overview of terrain and vegetation modeling, weather simulations, and modeling ecoclimates.

Vegetation Modeling. Modeling trees and plants has been content of computer graphics research for decades. A key objective of this research is to generate plausible and realistic branching structures of single plants and existing methods include fractals [Aono and Kunii 1984], repetitive patterns [Oppenheimer 1986], L-Systems [Prusinkiewicz 1986], and rule-based techniques [Lintermann and Deussen 1999]. On a different trajectory, data-driven approaches aim to reconstruct branching structures from images [Bradley et al. 2013; Li et al. 2021; Neubert et al. 2007; Quan et al. 2006; Tan et al. 2008], videos [Li et al. 2011], or laser-scanned point sets [Livny et al. 2011; Xu et al. 2007]. Furthermore, it has been recognized that user-defined sketches provide an efficient means to generate realistic plant structures, while also considering artistic requirements [Ijiri et al. 2006; Okabe et al. 2007; Wither et al. 2009]. More recently, methods aim to further improve the realism of plant models [Pirk et al. 2016] ranging from explicitly describing the environmental response of plants [Měch and Prusinkiewicz 1996; Palubicki et al. 2009; Pirk et al. 2012] to modeling with biological priors [Stava et al. 2014]. Previous work on plant dynamics ranges from modeling the growth process [Hädrich et al. 2017; Longay et al. 2012], successfully capturing biophysical and biomechanical deformations [Wang et al. 2013], and addressing plant plasticity [Zhao and Barbič 2013], to recent work on the machine learning-assisted acceleration of dynamic tree geometry [Shao et al. 2021]. Pirk et al. [2017; 2014] and Hädrich et al. [2021] introduce methods for coupling plant models with fluid dynamics to capture the growth response in wind fields and the combustion process of plants. Similar to these methods our goal is to couple detailed plant models with fluid dynamics, however, unlike them we focus on large-scale ecosystems.

Plant Ecosystems. Methods for generating models of plant ecosystems aim to jointly compute plausible distributions of plants and to represent plants with an appropriate level of geometric detail [Deussen et al. 1998; Lane and Prusinkiewicz 2002; Niese et al. 2022]. A number of approaches exists that represent plant ecosystems as layers [Argudo et al. 2017], voxels [Jaeger and Teng 2003], volumetric textures [Bruneton and Neyret 2012], through more principled level of detail strategies [Neubert et al. 2011], or based on simulating erosion feedback with vegetation [Cordonnier et al. 2017]. Furthermore, it has been recognized that the artistic authoring of ecosystems plays an important role [Beneš et al. 2009; Gain et al. 2017], which can even be facilitated based on neural networks [Kapp et al. 2020]. Furthermore, in forestry and ecology researchers widely explore stand-based, individual-based, and agent-based models of ecosystems at various scales of abstraction. The interested reader is referred to the surveys of Pretsch et al. [2008] as well as Zhang and DeAngelis [2020]. A related work to the method we propose can be found in Ch'ng [2011]. The work of Makowski et al. [2019] is the most advanced for simulating ecosystems with respect to climatic conditions and geometric representation of plants: different plant biomes are simulated based on individual, spatially-adapted plant instances and by considering temperature and precipitation

as the driving factors of ecosystem development and plant growth. In contrast to this work, our goal is to simulate the weather-based growth response of individual plants and – in turn – to also simulate the impact of vegetation on weather.

Weather and Cloud Simulations. Physics-based approaches for cloud modeling employ Eulerian solvers to advect fluids for simulating different forms of clouds [Harris et al. 2003; Herrera et al. 2021; Miyazaki et al. 2001; Overby et al. 2002]. Due to the importance of clouds in various application domains, there exists a number of representations for clouds that range from particles [Bouthors et al. 2008; Goswami and Neyret 2017; Neyret 1997], position-based dynamics [Ferreira Barbosa et al. 2015] to layers [Vimont et al. 2020], interpolation-based methods [Webanck et al. 2018], and cellular automata [Miyazaki et al. 2001]. However, despite these advances, simulating cloud dynamics remains a challenging research problem. Only very recently, Hädrich et al. [2020] proposed a physically-accurate solver for various cloud types and their formations that even enables the simulation of precipitation in the form of rain. In this work, we apply this solver to simulate the interaction of fluid dynamics and vegetation.

Vegetation Climate Response. Research in forestry, botany, and ecoclimates focuses on understanding the complex interplay of vegetation and climate. A number of methods investigate the impact of climate and weather on vegetation to explain the dynamics and functioning of plants, for example when exposed to climate warming [Liang et al. 2019; Zellweger et al. 2020]. Furthermore, climate can have a profound influence on the self-organization of plant ecosystems, which results in the formation of spatial patterns, such as labyrinths and gaps [Bastiaansen et al. 2020; Pringle and Tarnita 2017]. Conversely, it has also been recognized that vegetation affects weather and thus the climate. To understand this phenomenon, research focuses on establishing models that allow us to investigate the impact of vegetation on the water cycle and the climate system [Allan et al. 2020], heat transfer [Maréchal et al. 2010] as well as on understanding microclimate dynamics [Zellweger et al. 2020]. Vegetation defines a complex surfaces that interfaces with the weather system. Therefore, a number of methods investigate the impact of ecosystem composition on the formation of clouds [Horn et al. 2015; Xiao et al. 2018]. Many of the existing approaches aim at defining accurate models for ecoclimates. However most of these methods cannot be directly applied to geometric models of plants or be used to simulate the emerging phenomena of coupling weather and ecosystem at interactive rates.

3 OVERVIEW

Our main goal is to increase the realism of plant ecosystem models by simulating the interaction of vegetation, soil, and weather as shown in Fig. 2. The interaction of these models allows us to define ecoclimates and to simulate the water cycle (Fig. 3).

In our framework we have integrated and extended a tree growth model for large-scale plant ecosystems [Makowski et al. 2019]. Tree models are composed of a number of self-organizing branch modules that define the 3D branching structure of a tree model. Modules can be instantiated and are used multiple times across the same

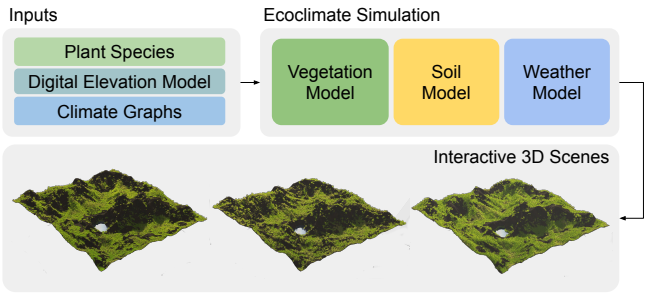

Fig. 2. Framework overview: we employ models for vegetation, soil, and weather to simulate ecoclimates. Our system operates at interactive rates and thereby allows users to efficiently explore configurations and parameters settings for plant species, terrain, and climate.

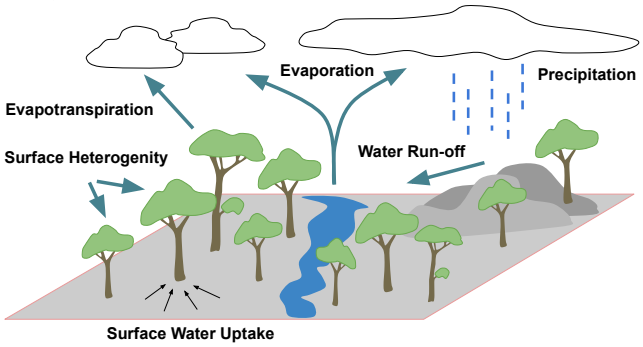

Fig. 3. We define ecoclimates by simulating the water cycle, including effects such as the water infiltration and water uptake of plants from the soil, the evaporation and transpiration of water from the ground and from leaves. Our model can realistically simulate the interaction of vegetation and fluid dynamics, resulting in complex microclimates.

tree as well as across other trees in the ecosystem. The advantage of this module-based representation is that it enables the efficient processing of large collections of plants. This means that we simulate the developmental process of the ecosystem as a collection of individually interacting plants, which results in unique and realistic branch geometry.

To simulate the atmosphere we integrated and extended a state-of-the-art method for simulating cloud dynamics [Hädrich et al. 2020], which allows us to capture various weather conditions and the formation of clouds. We couple the atmosphere and vegetation model by introducing a novel soil model. The soil model describes water infiltration into the soil as well as the water uptake by individual plants, which in turn can transpire water back to the atmosphere. Important to our work is that the coupling of fluid dynamics and plant ecosystems enables us to locally define the interactions of plants and weather – plants respond to the changes in the weather model, while the weather model is simultaneously affected by the vegetation. Sampling the weather over time establishes the climate for a simulated ecosystem.

In summary, we couple a module-based representation for vegetation with a state-of-the-art atmosphere model and a novel soil model for water infiltration. This allows us to model the feedback loops between vegetation, soil, and atmosphere to simulate essential ecoclimate phenomena.

4 ECOCLIMATES

Relatively recently earth's climate has been described by a system of several interacting spheres [Bonan 2015]. The main components of this earth system are the atmosphere (air), hydrosphere (water), cryosphere (frozen regions of earth), biosphere (living organisms), pedosphere (soil), and anthroposphere (humans). The major mediators between these different spheres can be defined by temperature and water in various phases. In this work, we emphasize the role of the climate on the biosphere: the **ecoclimate**.

In the atmosphere, water undergoes phase transitions between condensed form and rain. When liquid water reaches the ground as rainfall some of it drains downward due to the force of gravity. This vertical flow of water is called **infiltration**. The water that infiltrates into the soil is stored as **soil water**. When the infiltration capacity of soil is exceeded, water collects as puddles in small depressions of the ground surface. When these are filled, water runs off over the ground surface as overland flow. Soil water returns to the atmosphere through **evaporation** from bare ground and **transpiration** from plants. Evaporation is understood as the physical process by which water turns from liquid to vapor in the air. Transpiration is evaporation of water held inside plants. Due to the difficulty in clearly separating these processes, they are also jointly referred to as **evapotranspiration**. Plants consume large amounts of water during growth. However, plants cannot grow if leaf pores (stomata) are not open. In case stomata have opened, water contained in the leaf may diffuse out as transpiration. If too much water is lost, the plant becomes desiccated and will die in case its internal water is not replenished through the roots from water in the soil. Therefore, plants have to compromise between the need to transpire and grow, and to prevent water loss and not grow.

The complexities of the hydrologic cycle on land can be reduced to a simple form in which the change in soil water (Δq_w) is the balance between water input from rainfall (R), water loss from evapotranspiration (E), and water lost as runoff (q_o). This cycle has a major impact on vegetation growth patterns, such as **spatial self-organization** of plants due to climate variations, **forest edge effects** which are defined by stark climatic gradients, and the influence of the topography on vegetation (**geomorphic effects**).

Conversely, wet soil or dense vegetation matter creates a cool, moist atmospheric boundary layer which may feed back to increase precipitation. In addition, rough surfaces such as forests generate more turbulence of air flow compared to smoother surfaces such as grasslands. A smoother surface can lead to a warmer, drier atmospheric boundary layer and therefore to different cloud formation. The surface characteristics of a given geographic location are described as **surface heterogeneity**. This bidirectional coupling of ecosystems and climate occurs over a continuum of timescales from minutes to seasons to millennia.

5 MODEL

For a realistic 3D simulation of ecoclimates we formally describe cloud formation and plant growth at a detailed geometric scale. Our ecoclimate model is distinguished by a vegetation model based on space-constrained plant growth (Figure 6a), a soil model describing terrain hydrology (Figure 6b), and a weather model simulating fluid dynamics (Figure 6c).

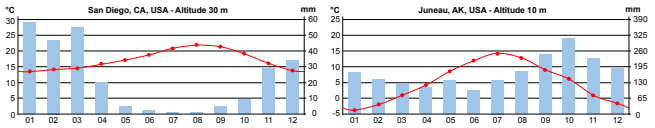

Fig. 4. We use the monthly average temperature (red) and precipitation (blue) as input to our framework. Two different temperature and precipitation graphs for San Diego and Juno shown as example inputs.

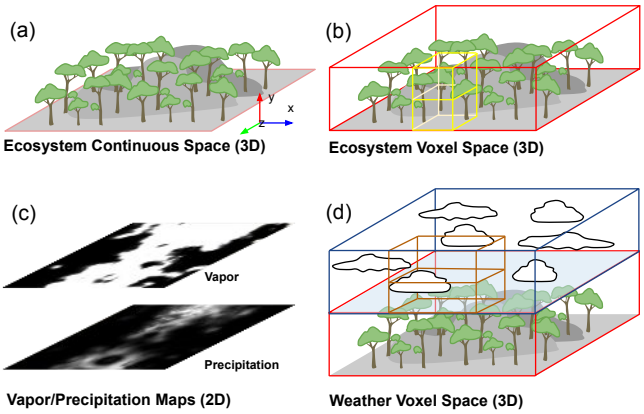

Fig. 5. Mathematical spaces used in our framework. We use a continuous space to embed terrain surface and vegetation meshes used for 3D rendering (a); a discrete 3D grid composed of cubic voxels to store temperature and light information relevant to computing ecosystem development (b); a vapor and precipitation map to transfer data about water and temperature between individual models of our method (c); and a discrete 3D grid composed of cubic voxels for calculating the dynamics of fluid motion (d).

5.1 Spaces

To simulate ecoclimates based on the vegetation, soil, and weather models we rely on four different spaces as illustrated in Fig. 5. First, we define a continuous 3D space in which we embed a digital elevation model and vegetation geometry that is suitable for 3D rendering (Ecosystem Continuous Space). For most of our scenes we define terrains of size 4 km^2. Second, we use a 3D voxel space with a resolution 1.5 m to compute light exposure and temperature values to express plastic development of plants (Ecosystem Voxel Space). Third, we define 2D grids with a resolution 1.5 m to store values for average monthly vapor and precipitation over the terrain (Vapor and Precipitation Maps). Finally, we use a 3D voxel space with a resolution 20 m for our cloud simulation (Weather System Voxel Space). Exchange of water quantities between *Weather Voxel Space (WVS)* and *Ecosystem Voxel Space (EVS)* is facilitated via vapor and precipitation maps. The use of precipitation and vapor maps to express components of the hydrological cycle instead of operating on the respective 3D grids improves the computational efficiency of our method. The local storage of water, light exposure and temperature values defines the microclimate in our method.

5.2 Input and Output

Our framework allows us to interactively explore ecoclimates. To define an ecoclimate a user can specify a terrain (digital elevation model) and a set of plant species. We use the the method of Makowski et al. [2019] to design a set of plant species P. This method

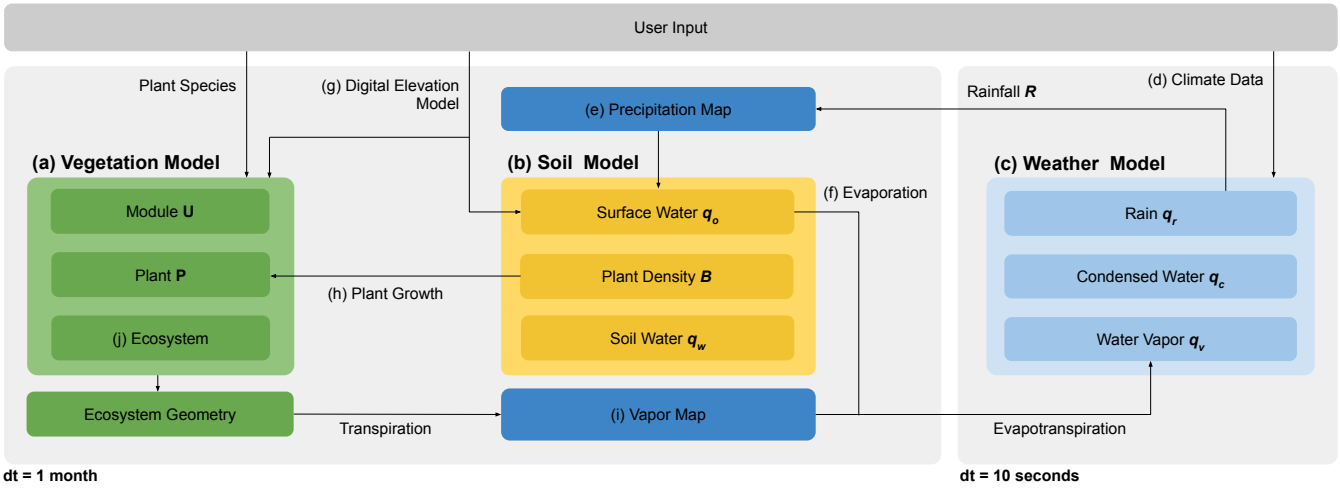

Fig. 6. Detailed overview of our ecoclimate model. Our model can be distinguished by a vegetation (a), soil (b), and weather model (c). We explicitly describe the water cycle which mediates the feedback between the three models. While the weather model describes dynamic cloud formation over time scales of seconds the vegetation and soil model describe phenomena occurring on time scales of months. A user provides input in the form of a set of plant species, a digital elevation model and data describing macroclimatic variation over time. A description of the processes that our model is able describe and the underlying hypotheses expressed by our ecoclimate model is given in Section 5.3.

requires setting a number of parameter values that define plant growth in an ecosystem, such as for shade tolerance, precipitation and temperature adaptation.

A macroclimate is defined as a set of monthly average values for temperature and precipitation describing climatic variation during an average year. Examples of two macroclimates for different geographic locations are shown in Fig. 4. Moreover, a user can specify a wind field that defines additional input for the fluid dynamics. Our framework allows to specifiy a wind vector f_w applied to all grid cells of the *Weather Voxel Space*. The wind field can either be defined manually or obtained from online weather services as shown in Hädrich et al. [2020].

The output of our algorithm is terrain surface mesh and a set of 3D plant models with their geometry adapted to their environment. Plant models are defined as sets of branch modules which are used multiple times across the same plant and within the entire ecosystem. Each module is individually adapted to its location in the plant and its geometry is generated on the GPU. This way modules can be instantiated, which facilitates the efficient rendering of large plant collections. In addition, condensed water q_c in the *Weather Voxel Space* is rendered as clouds using volume ray marching.

5.3 Hypotheses

We aim to create an ecoclimate model that expresses realistic vegetation growth and cloud dynamics, as well as the feedback loops between them. This feedback is mediated by water and temperature quantities stored in the *Ecosystem Voxel Space*, vapor and precipitation maps, and the *Weather Voxel Space*. In the following we list the major hypotheses described by our formal model:

(1) Water is treated as an extensive quantity that can vary according to global weather influx as defined by the macroclimate input (Fig. 6d, Sec. 5.7).
(2) Water in the atmosphere undergoes phase transitions between vapor q_v, rain q_r, or in condensed form q_c as proposed by the Kessler scheme [1969] (Fig. 6c, Eqs. 10, 11, 12).
(3) Rain R increases the amount of surface water q_o (Fig. 6e, Eq. 7).
(4) Surface water q_o moves by diffusion, is advected by the slope of the terrain v, evaporates back into the air as q_v, and can infiltrate into the soil (Fig. 6b, f, g, Eq. 7).
(5) Water infiltration into the soil is proportional to the density of plants B (Fig. 6b, Eq. 6).
(6) Plants P take up soil water q_w and transpire it as q_v to grow (Fig. 6a, h, i, Eq. 6).
(7) Plant growth is expressed by competition for light, apical control, tropisms, flowering, climatic adaptation, shade tolerance and seed dispersal (Fig. 6i). For a more detailed explanation please see Makowski et al. [2019] (Secs. 5.2-5.3, 6.1-6.4).
(8) Plants P decrease light exposure and temperature (Fig. 6j, Sec. 5.5.1). For a more detailed explanation please see Makowski et al. [2019] (Sec. 6.2).

Hypotheses (1-5) are described by partial differential equations. Whereas, hypotheses (6-8) are described by a discrete, graph-based method. Both the continuous and discrete formalism exchange quantities between each other. Specifically, the density of plants B is computed from the number of plants P and the growth of plants P is modulated by the soil water q_w. This means that we use a coupled continuous and discrete formalism to describe the major empirical hypotheses underlying our ecoclimate model.

5.4 Time Scales and Model Integration

It is important to note that our ecoclimate model operates on two different timescales. The simulation of vegetation development and water cycle in the soil takes place at a timescale of one month Δt_E (Fig. 7 indicated by green horizontal line). This timescale allows

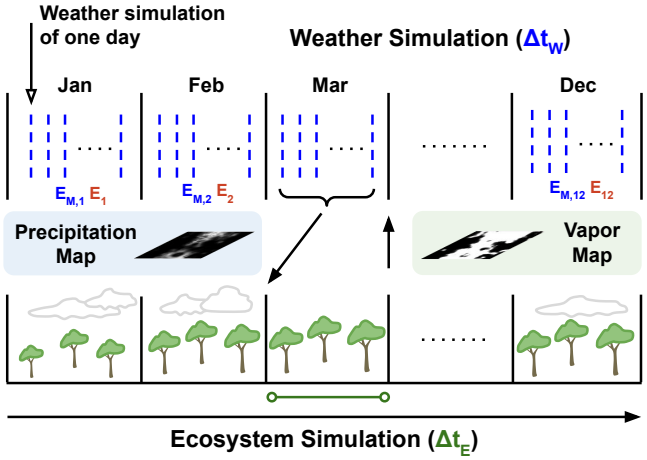

Fig. 7. We simulate ecoclimates at two time scales. First, we sample daily weather conditions by simulating weather over a period of time at a time step of 10s (dashed blue lines). Second, we obtain a precipitation map to represent the monthly weather conditions by simulating weather for a number of days each month. These monthly average weather conditions are used as input for the ecosystem simulation which uses a time step of one month (green line). After a step of ecosystem simulation we compute a vapor map as input for the subsequent month of weather simulation.

us to simulate the long-term development of plant ecosystems and consequently the vapor maps necessary for computing corresponding weather variations for a given month. To simulate the annual variation of climate, we define 12 unique weather conditions for each month by defining macroclimatic vapor and heat emission (Sec. 5.7). For each month we simulate weather at a small time scale (10s-60s) until we obtain a plausible sample of the local weather conditions for a given day. Sampling monthly weather multiple times allows us to obtain an average temperature and precipitation profile for a given ecosystem (Fig. 4) that we store as a precipitation map (Fig. 7). The partitioning of monthly weather simulation into batches of individual days allows us to use plausible precipitation profiles for a given ecosystem. The coupling of weather and ecosystem simulation based on maps of precipitation and vapor defines the ecoclimate feedback loop in our model.

5.5 Vegetation Model

We use the method introduced in Makowski et al. [2019] to model vegetation development. This method allows modeling the growth of a large number of interacting plant instances while maintaining an individual, geometric representation at branch scale. Furthermore, this method also describes climatic adaptation, shade tolerance, and seed dispersal strategies to place plant models realistically into an environment.

A plant model in our simulation is represented as an ordered tree graph of connected modules $u \in U$ (plant graph) embedded in a continuous 3D space representing the environment and a set of plant type parameters χ – altogether this defines a plant P. A module represents the skeletal graph (defined by nodes $c \in C_b$) of a branch cluster. During simulation time we express plant development by modifying the plant graph through adding, removing or adjusting

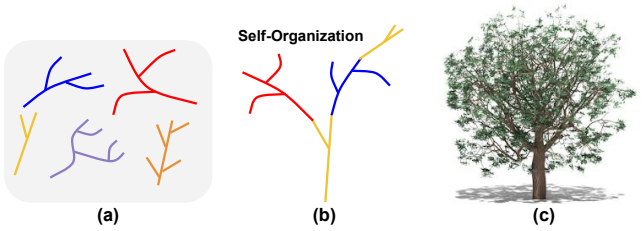

Fig. 8. Module-based plant representation: plants are composed from a set of modules (a). Modules adapted through self-organization and are reused across the same plant and the entire ecosystem (b). Once the branch graph has been defined we generate the final plant geometry as illustrated in (c).

modules. At each simulation step we calculate plant development based on light exposure values obtained for each module to express constraints of space and to avoid module collisions. When new modules are added to the plant graph they are interpolated from an axiomatic developmental stage (a single branch segment) to a maximally developed stage. The maximally developed stage is defined by one of nine pre-defined branch templates (as illustrated in Fig. 8).

To express the invasion of foreign species that did not start in the initial scene we place, with uniform distribution, seeds of other plant types at fixed time intervals (global seeding). We compute a climatic adaptation parameter o that scales the global seeding interval for all plant types defined for the scene:

$$o = \frac{\mathcal{N}_T(T) \cdot \mathcal{N}_P(q_w)}{\mathcal{N}_T(T_A) \cdot \mathcal{N}_P(P_A)}, \tag{1}$$

where $\mathcal{N}_T(\cdot)$ and $\mathcal{N}_P(\cdot)$ denote the normal distributions of local temperature (mean is T) and local soil water (mean is q_w) which are obtained by reading the values from the voxel cell where the plant is located (*Ecosystem Voxel Space*). In contrast to Makowski et al. [2019] (Sec. 6.4), where global temperature and precipitation values are used to linearly interpolate the maximum value of vigor (v_r) by o, our local sampling enables simulating microclimates.

5.5.1 Calculating Vapor Maps. In the final step of a cycle of the development of vegetation we calculate vapor maps which are used as input data for the weather model (Fig. 9, b). We project all modules into a 2D grid. Then each grid cell that contains the geometric center of a module is updated with its biomass, scaled by a transpiration coefficient τ to define a final vapor value E_p at this cell

$$d_b = \begin{cases} \sqrt{\sum_{c \in C_b} d_c^2}, & C_b \neq \emptyset, \\ \phi, & \text{otherwise}, \end{cases} \tag{2}$$

$$\ell_b = \min(\ell_{\max}, \beta \cdot a_b), \tag{3}$$

$$M_m = \sum_{u \in U} \sum_{c \in C_b} \ell_b (2 d_b)^2 \pi \rho, \tag{4}$$

$$E_p = \tau \sum_{u \in U} M_{m,u}. \tag{5}$$

where d_b denotes branch segment diameters, a_b the age of a branch segment, ℓ_b branch segment lengths, and M_m the total mass of a

module u. β is a scaling coefficient. $\ell_{\max}$ the maximum length a branch can attain and ρ the average wood density. This process describes the amount of evapotranspiration over the terrain during a period of growth in our method. Furthermore, we define the cooling of air induced by plants by linearly interpolating the weather temperature to a minimum temperature T_{sh} in complete shade by the light exposure value Q of the *Ecosystem Voxel Space*. This linear interpolation of Q values represents a coupling of the *Weather Voxel Space* with the *Ecosystem Voxel Space*. Both voxel spaces are embedded in the *Ecosystem Continuous Space* which allows us to coherently sample them.

5.6 Soil Model

Our soil model expresses the change of soil (∂q_w) and surface water (∂q_o) due to precipitation (R), and the plant density (B). The model describes the interaction between the available water and the vegetation (Fig. 9, a). This interaction occurs on different time scales between the spreading of water and of vegetation growth which leads to spatial vegetation patterns. The soil model is defined by a set of partial differential equations which are coupled to the dynamics of the discrete vegetation growth model. It is therefore neither continuous nor discrete but instead represents a hybrid modelling approach. The differential equations are:

$$\frac{\partial q_w}{\partial t} = \alpha \cdot q_o \cdot \frac{B + k_2 \cdot W_0}{q_w + k_2} - g_{\max} \cdot \frac{q_w}{q_w + k_1} B \\ - r_w \cdot q_w + D_w \cdot \Delta q_w \,, \tag{6}$$

$$\frac{\partial q_o}{\partial t} = R - \alpha \cdot q_o \cdot \frac{B + k_2 \cdot W_0}{q_w + k_2} + D_O \cdot \Delta q_o + v \nabla q_o \,, \tag{7}$$

where $g_{\max}$ is the maximum water uptake, k_1 is a half-saturation constant of water uptake, α is the maximum infiltration rate, k_2 is the saturation constant of water infiltration, W_0 is the water infiltration rate in the absence of plants, r_w is the specific soil water loss due to evaporation and drainage, D_w is the diffusion coefficient for soil water, R is precipitation (Sec. 5.7.2), and D_O is the diffusion coefficient for surface water. Plausible parameters were obtained from the literature [HilleRisLambers et al. 2001; Rietkerk et al. 1997] A Laplacian operator is used to express water diffusion. We account for the slope of the terrain to model water runoff by adding an advection terms $v\,\nabla q_o$, in which v represent the downhill flow. The two-dimensional numerical simulations are solved using the forward Euler integration scheme resulting from the spatial discretization (precipitation map) of the diffusion operator.

In each simulation step, the plant density B (Eq. 6–7) of each grid cell is calculated by summing the biomass values of all the plant models P_i located in this cell. The plant models P_i are defined by the vegetation model in Section 5.5:

$$B = \sum_{P_i \in P} \frac{P_{m,i}}{A} \,, \tag{8}$$

$$P_{m,i} = \sum_{u \in U} M_{m,u} \,, \tag{9}$$

where $M_{m,u}$ is the mass of module u of a plant model P_i, and $P_{m,i}$ the total biomass of the plant, and A the area of a side of a voxel cell. This coupled continuous and discrete model exhibits a Turing-like

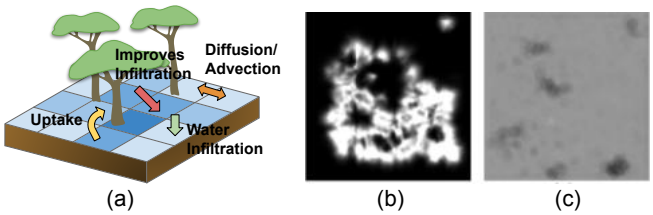

Fig. 9. Our model describes the interaction between the available water and the vegeation (a). We define maps to store the average monthly vapor (b) and precipitation (c) of a terrain. Based on these maps we define the exchange of water quantities between the *Weather Voxel Space* and the *Ecosystem Voxel Space*.

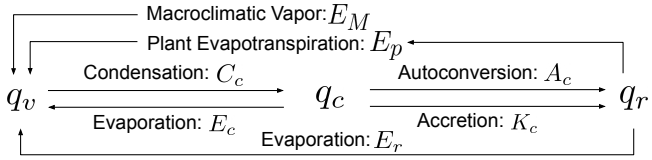

Fig. 10. Illustration of our extended Kessler's scheme [1969] for modeling the transport between surface water, soil water, vapor, cloud water, and rain.

mechanism similar to the continuous model proposed by HilleRis-Lambers et al [2001]. It is characterized by a short-range negative feedback and a long-range positive feedback of vegetation on itself (Eq. 6). Please note that these type of reaction-diffusion models are used to describe a variety of pattern formation, e.g. pigmentation patterning in flowers [Ringham et al. 2021].

5.7 Atmosphere Model

Our weather model is based on the method described in Hädrich et al. [2020] which includes additional derivation steps of the equations introduced here. This method enables a realistic simulation of the exchange of water, vapor, and heat between parcels of air and the terrain. Furthermore, it captures turbulent air flows enabling the simulation of a range of phenomena such as stormscapes and dynamic transitions between different cloud types.

Our weather model can be divided into an atmospheric model that describes temperature and pressure changes as a function of altitude and time, a 0D thermodynamics model that defines local forces and the formation of clouds, and the fluid dynamics model defining the motion of air in the atmosphere. The complex terrain-cloud feedback in the original method is expressed by noise functions defining ground vapor and heat values introduced at the bottom domain boundary of the fluid field. These functions are scaled by vapor V and heat emission E. Here, we extend the notion of ground vapor and heat by assuming that vapor and heat can be added from any boundary to the fluid domain to represent influx from the macroclimate. We refer to this vapor and heat as macroclimatic vapor E_M and heat E. Unlike Hädrich et al. [2020] the cloud-terrain feedback is expressed in our model by the *Ecosystem Voxel Space* and the vapor maps generated by the soil and vegetation model. We add macroclimatic vapor E_M and evapotranspiration E_p stored in the vapor maps to the boundary of the *Weather Voxel Space*.

5.7.1 Fluid dynamics. To account for phase transitions of water in the air, i.e. from water vapor q_v to condensed cloud q_c, and rain

Fig. 11. We varied macroclimatic parameters of vapor and temperature to approximate different cloud types for the same ecosystem scene. This includes clouds types such as stratocumulus, stratus, and cumulus.

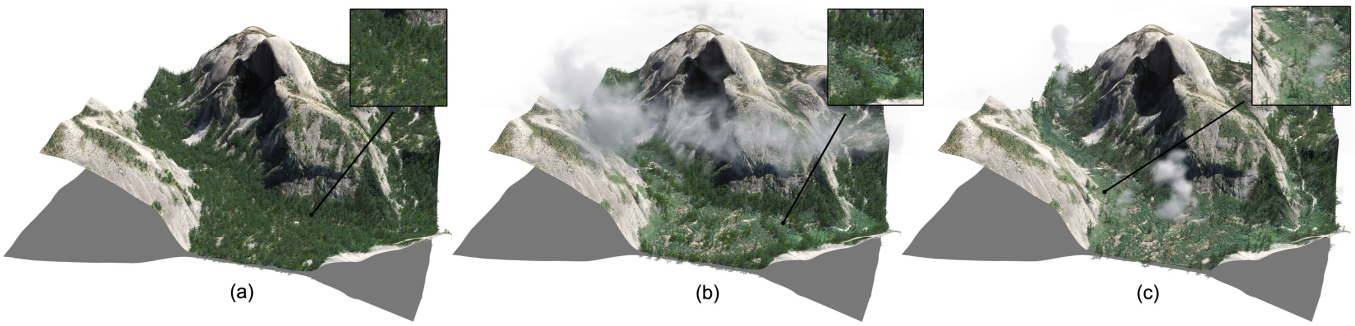

Fig. 12. Forest growth in the terrain around Half Dome in the Yosemite National Park: We simulate an ecoclimate with a dense population of pine trees (a). We then modify vapor values and continue growing the forest to simulate climate change. Typical ribbon-like structures emerge due to spatial patterning of plants (b). Finally, severe forest dieback occurs resulting in an arid landscape with fewer an feebler trees (c).

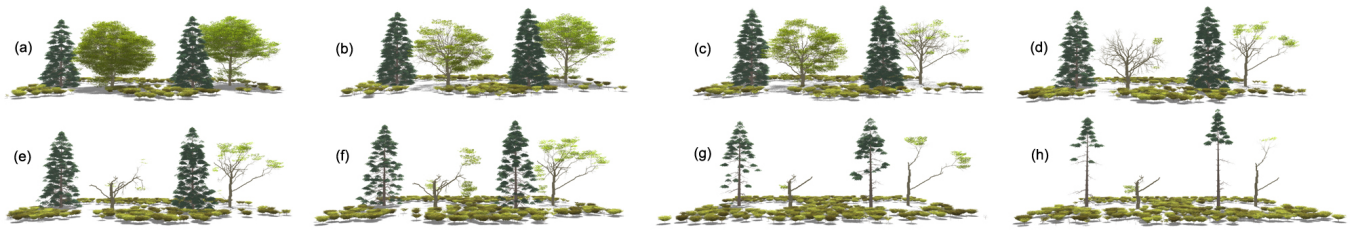

Fig. 13. Illustration of climate change for a small vegetation patch: our approach represents trees with individual branch geometry, which allows trees to individually adapt to a changing climate. From initially beneficial conditions (a), we gradually decrease average precipitation from 1200 mm to 100 mm (b-h). The more precipitation-adapted oak trees exhibit changes to its architecture before the less precipitation-adapted pine trees. After shedding most of its branches the oak trees continue to adapt to the drier conditions growing even under severe water stress (e, f). Shrubs continue to grow throughout the drought conditions as they are highly adapted to either climate.

q_r, we extend Kessler's methodology [1969]. Using the material derivative $\mathrm{D}_t\varphi = \partial\varphi/\partial t + \boldsymbol{v}\cdot\nabla\varphi$ [Kundu et al. 2012], the transport equations are

$$\mathrm{D}_t q_v = -C_c + E_c + E_r + E_p + E_M\,, \tag{10}$$

$$\mathrm{D}_t q_c = C_c - E_c - A_c - K_c\,, \tag{11}$$

$$\mathrm{D}_t q_r = A_c + K_c - E_r\,, \tag{12}$$

where the source term C_c denotes condensation, E_c the evaporation of clouds, E_r the evaporation of rain from the ground, A_c autoconversion of raindrops from clouds, K_c the accretion of cloud water due to falling water drops, E_M the macroclimatic vapor, and E_p the evapotranspiration of plants. E_M is calculated from the macroclimatic vapor function and E_p is obtained from the vapor maps. E_p and E_M are non-zero only at the domain boundary (representing the terrain). Fig. 10 illustrates the phase transitions of water encapsulated by this model. Please refer to the derivation of the source term C_c, the remaining variables, as well as the numerical implementation to Hädrich et al. [2020].

5.7.2 Calculating Precipitation Maps. To simulate the yearly variation of weather over a terrain we rely on our weather model to generate precipitation maps (Fig. 9c). These maps contain the input for the soil model describing the hydrological cycle on the ground. This provides us a detailed enough description to express a variety of microclimatic phenomena (e.g. forest edge effects). The macroclimatic parameters for the corresponding time in the year are obtained using the climate interpolation functions p_0 and T_0. Next, we simulate cloud formation for a fixed number of time steps, e.g. 10-100 steps. We then project the rain values q_r of each cell from top to bottom (a column in voxel space) of the grid as rain R into the precipitation map:

$$R = \sum_{q_r \in Q_r} q_r\,. \tag{13}$$

The variable R is used to compute the surface water q_o (Eq. 7). This process is repeated a number of times for each month to express a daily variation of weather conditions. To express this idea formally we sample a normal distribution of E_M and θ once for each day to

finally obtain an average precipitation map for the given month. We compute 12 average precipitation maps representing the monthly rainfall over a year by using 12 sets of macroclimatic parameters (T_0, p_0) based on a climate graph (Fig. 4).

6 IMPLEMENTATION DETAILS

We have implemented our interactive framework using C++, DirectX and CUDA. To generate the results shown in this paper we used an Intel(R) Core i5, 4 x 2.5GHz with 6GB RAM, and a NVIDIA Geforce GTX 1050 GPU (4 GB RAM). We used the L3DT Terrain Editor to generate terrain meshes. The figures shown throughout the paper are rendered with our interactive OpenGL-based framework. Tab. 2 reports configuration settings, parameter values, and simulation times. Details about the plant types are provided in Tab. 1. We evaluate the performance of our method in Appx. C.

Joining models expressed with different formalisms, namely the continuous formulation of soil and weather with the discrete representation of vegetation is a non-trivial implementation task. At the beginning of each update step, we compute a set of parameter values for the weather simulation runs that will serve to represent annual weather conditions (Alg. 1, Lines 2-4). We then simulate for each instance of climatic conditions ψ a weather scene (Alg. 1, Lines 5-10). For the implementation of the fluid solver we rely on the integration scheme described in Hädrich et al. [2020], which includes diffusion, advection and pressure projection (Alg. 1, Lines 5-10).

The WVS is used to store all relevant quantities representing the state of the weather simulation. For the advection process, we employ no-slip conditions at the bottom and free-slip conditions at the ceiling. The vertical velocity is set identically to zero at the side boundaries and if an external wind field is specified, the horizontal velocities are computed as the corresponding wind speeds.

We provide the input for the soil simulation in the form of 2D precipitation maps obtained from the WVS (Alg. 1, Line 10). The soil is represented by two 2D grids representing the surface and soil water. We use Eulerian solvers to compute the diffusion and advection of water [Stam 1999] based on the input of rain R obtained from the precipitation map (Alg. 1, Lines 11-14). We use free-slip conditions at the boundaries.

Next, we compute the light exposure values for the EVS. After computing local light and soil water values we initiate the growth simulation of vegetation for all plants P of a scene $\mathcal{S}$ (Alg. 1, Lines 11-14). First, we compute v_r based on the climatic adaptation parameter o which is obtained from the local temperature T and soil water q_w as described in Eq. 1. Then, we traverse all modules (M) of a plant P to compute their state changes, as well as orienting and positioning plant modules using stochastic gradient descent (Alg. 1, Lines 18-22) as outlined in Makowski et al. [2019]. Finally, we update vapor and temperature values in the WVS based on the new state of the vegetation simulation and seed new plants in the scene (Alg. 1, Lines 24-27).

7 RESULTS AND EVALUATION

In this section we describe how our ecoclimate framework can be used to model highly complex and realistic landscapes. As we are proposing a large parameter space our main goal is to carefully validate our results based on a range of different experiments that assess the impact and usefulness of each of the introduced models – atmosphere, soil, vegetation. The main advantage of our model, compared to other approaches that consider modeling the macroclimate (e.g. Makowski et al. [2019]), is the simulation of a microclimate. Consequently, we can generate more realistic landscapes with a larger variety of ecoclimate phenomena. We consider our method to be interactive, meaning we generate all results with frame rates high enough to allow for a fast response of the simulation to user interaction. Finally, we compare our simulation results to recent theoretical studies of climate change and real world examples.

ALGORITHM 1: Overview of our numerical procedure.

```
Input: Current system state.
Output: Updated system state.
1  Procedure:
2    for each γ ∈ Γ do
3    | Compute normally distributed pair of E and E_M as vector v
4      based on annual climate profile as described in Sec. 5.4.
5    for each ψ ∈ Ψ do
6    | Update atmospheric temperature T(x). Diffuse, advect and
7      pressure project temperature θ, field u and atmospheric
8      water content q_j following the Eulerian solver
9      of Hädrich et al. [2020].
10   | Update precipitation map as described by Eq. (13).
11   Compute water transfer between soil surface
12     and atmosphere as explained in Eq. (5).
13   Compute water exchange between surface, soil and plants
14     as explained in Eqs. (6), (7).
15   for each P ∈ S do
16   | Update Light exposure values in EVS according to shadow
17     propagation algorithm as described in Makowski et al. [2019].
18   for each P, M ∈ S do
19   | Compute v_r as explained in Eq. (1).
20   | Compute vigor values for all modules, shed branches and remove
21     plants, update module positions and orientations using SGD, as
22     described in Makowski et al. [2019].
23   for each P ∈ S do
24   | Update vapor values E_P in WVS as described in Sec. 5.5.1.
25   | Update temperature values T in WVS as described in Sec. 5.5.1.
26   | Seed new plants as described in Makowski et al. [2019].
27 end
```

7.1 Ecoclimate Dynamics

Jointly simulating the soil, vegetation, and atmosphere models generates feedback loops that allow us to capture climate change effects mediated by the water cycle. Specifically, we show that our atmospheric model is able to represent different climatic conditions by providing examples of a variety of cloud formations. We also establish that the dynamics of the atmosphere affect the development of the vegetation model. Conversely, we show that the development of vegetation influences the atmospheric conditions which – in turn – may lead to changing cloud formations.

7.1.1 Atmosphere. Similar to previous results on cloud formation [Hädrich et al. 2020] we also simulate cloud dynamics. Unlike the

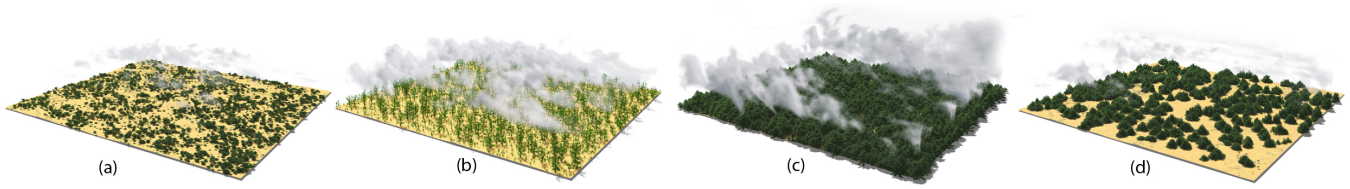

Fig. 14. Results of evapotranspiration from vegetation: we set microclimatic parameter values constant in four different biomes. The plant species determines the evapotranspiration rate of a plant leading to different cloud formations in a shrubland (a) and a patchy oak forest (b). In (c) we show denser cloud formations over a pine forest; by reducing the density of pines less vapor is available for cloud formation (d). Please note that clouds in the images are rendered at low altitudes for visualization purposes.

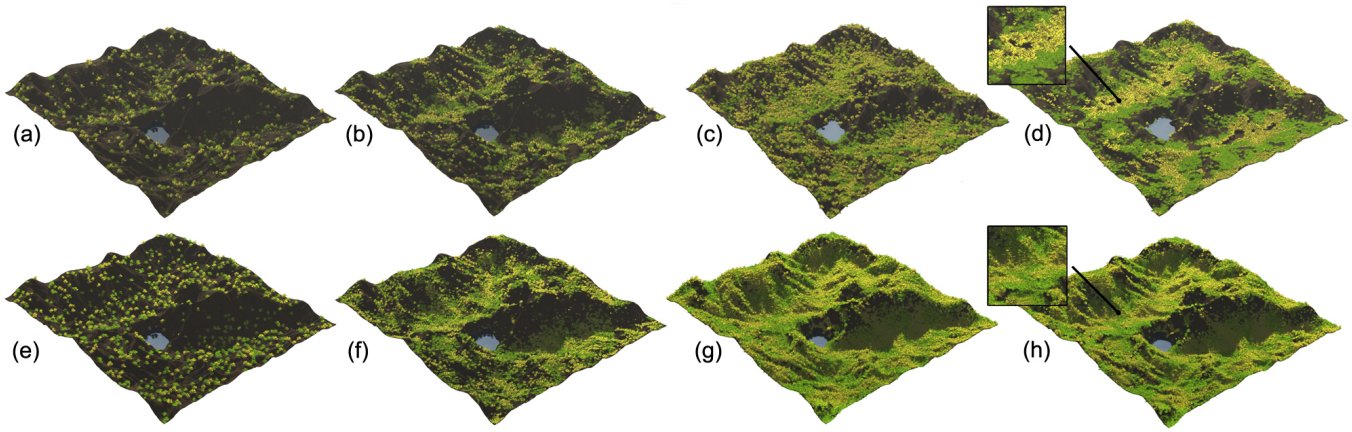

Fig. 15. Comparison to [Makowski et al. 2019]: Temporal progression of a developing ecosystem composed of a drought-adapted green-leaved and a yellow-leaved species generated with microclimates (a-d) and without microclimates (e-h). The inclusion of microclimates allows for more realistic patterning of vegetation at the slopes of the terrain capturing geomorphic effects. Additionally, patterns of self-organization emerge as the yellow-leaved species establishes itself primarily in the valleys of the terrain after water infiltration is sufficiently improved through the presence of the green-leaved species (top row): a case of plant cooperation (d and h, inset).

previous work we couple our vegetation and atmosphere models through a dynamically computed vapor map, which allows us to establish the necessary feedback loop between vegetation and atmosphere. In Fig. 11 we vary parameter values for vapor and heat emission of the macroclimate over the same boreal forest patch. This parameter space exploration results in the formation of different cloud types ranging from foggy clouds to stratocumulus and cumulus clouds. For this experiment we extended the model of Häedrich et al. [2020] by using a vapor map obtained from the vegetation simulation, described in Section 5.5.1, instead of a vapor map defined by a noise function.

7.1.2 Atmosphere-Vegetation. Our framework allows us to simulate the impact of the atmosphere on the vegetation. The interaction between atmosphere and vegetation models is defined by a precipitation map, which is used to provide soil water necessary for vegetation growth. This means, that changing atmospheric conditions of macroscopic vapor will impact vegetation development. In Figure 12 we demonstrate the atmosphere-vegetation feedback by simulating an ecoclimate in the Yosemite Valley around Half Dome (a) resulting in a dense population of pine trees (a, inset). Reducing the macroscopic vapor leads to a reduced availability in soil water resulting in forest dieback (b). In this case, ribbon-like structures of pine trees emerge as result of this climate change (b, inset). Further decreasing the vapor eventually causes more trees to die (c), which leads to an arid landscape with fewer and feebler trees (c, inset).

The visual forest patterns emerging due to changing climatic conditions are very complex. In Fig. 24 we show the transition of a tropical forest to an arid landscape by reducing the macroscopic vapor gradually with simulation time. The tropical forest is characterized by 6 species which are organized in a mixed stand (a). As precipitation decreases to 3700mm the less well-adapted tree species die back forming large forest gaps (b). This allows fast growing and more climate-adapted species to proliferate, changing the forest composition in the process (c, 2500mm). As the climate further changes plant species segregate to exploit climatic niches on the terrain (d, 1260mm). Finally, continued decrease of precipitation results in arid vegetation pattern.

In Fig. 13 we show a close-up simulation of a changing climate on a smaller patch of vegetation consisting of oaks, pines and shrubs. Our framework specifically models both the above-ground as well as below-ground interactions between different plants. This allows us to generate vegetation structures with unique geometries adapted to their local environment. For example, in (a) - (d) the right oak tree sheds its left facing branches first due to the shade of the nearby pine tree. Furthermore, after the oak trees lose most of their branches and their shade impact vanishes, shrubs grow into the space with the now better light conditions (g) - (h). These detailed above-ground

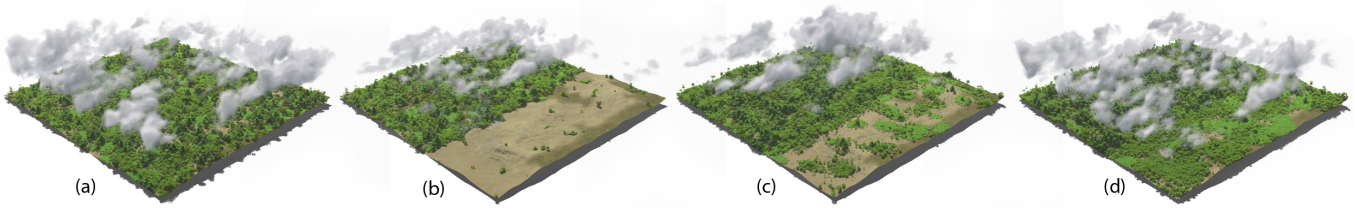

Fig. 16. Our method models the feedback between vegetation, soil, and weather. To illustrate this, we conduct a deforestation experiment while keeping the macroclimate in our weather model constant. In (a) we show a tropical rainforest with cumulus clouds. In (b) we remove a large portion of the rainforest thereby modifying the vapor emission from the terrain. Consequently, fewer cumulus clouds form, especially over the deforested area. After continuing ecosystem growth cloud formation increases slightly (c). Only after significant portions of the rainforest have regrown, cumulus cloud formation is restored (d). Please note that clouds in the images are rendered at low altitudes for visualization purposes.

vegetation interactions could not be simulated by soil-mediated interactions due to the coarseness of the precipitation and evaporation maps.

7.1.3 Vegetation-Atmosphere. To validate the impact of vegetation on the atmosphere we conducted the following experiment: we selected four different ecosystems with the same atmospheric conditions – parameter values are identical across all scenes. Then, we simulated the atmospheric model for the exact same amount of steps of weather simulation. Figure 14a shows an arid shrubland comprised by a species with a low evaporation rate. In this case, only a small, faint patch of clouds is forming over the terrain. In contrast, a young oak forest with a high evaporation rate generates more visible clouds as depicted in Figure 14b. In Figure 14c, d we created two different pine forests with the same evaporation rate. The overall higher biomass of the denser pine forest (Figure 14c) results in higher vapor values in the vapor map and consequently in the formation of cumulonimbus clouds. In contrast, the sparser pine forest with overall lower vapor values generates only faint cloud formation (Figure 14d). These results showcase the feedback of vegetation on the atmosphere via plant evaporation rates and biomass.

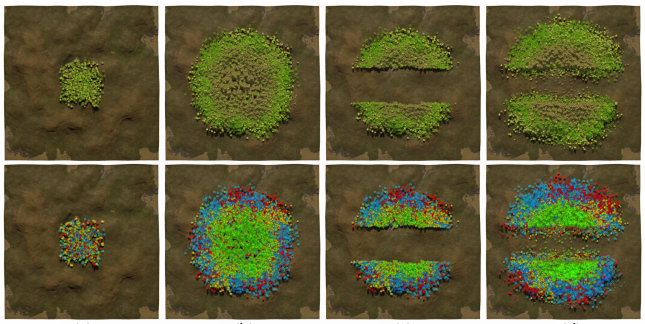

Fig. 17. A mixed stand forest patch emerging from centrally distributed seeds of four different species (a). After further simulation a climax species establishes itself in the center of the forest patch with the remaining species at the forest edges due to microclimates (b). We interactively cut back trees to fragment the forest into two patches (c). After several years plants grow back into the gap with similar species distributions at the edges as before the disturbance (d). Our microclimate model realistically captures increasing edge effects due to forest fragmentation. In the bottom row we visualize plant species with colors red, blue and yellow for edge species and green for the climax species.

7.2 Microclimate

The main motivation behind our ecoclimate model is to describe the feedback loops between soil, atmosphere and vegetation locally. Therefore, all spaces used to represent the soil, atmosphere and vegetation components of our ecoclimate model are described by grids. This local representation allows us to express spatial gradients of temperature, light availability and water representing the microclimate. In contrast to a global definition of climatic parameters such as used in [Makowski et al. 2019], this enables simulating various important phenomena controlled by the microclimate. We demonstrate the usefulness of a local, bidirectional vegetation-soil feedback by simulating the effects of topography of vegetation growth and the plausible vegetation growth dynamics at forest edges. Furthermore, we present the Foehn effect as an example of how a local description of the atmosphere allows modeling realistic vegetation distribution along mountain sides. Finally, we show how deforestation can locally affect the atmosphere by changing cloud formation dynamics.

7.2.1 Geomorphic Effects and Plant Cooperation. Our method emergently expresses the effects of the topography on vegetation growth via the hydrological cycle. In Eq. 7 of the soil model we describe the diffusion and run-off of surface water based on ground slopes. Water infiltration is diminishing with the steepness of slopes. Consequently, this means that plant development is affected by the geomorphology of the terrain – more water is available in terrain crevasses. Therefore, soil water can establish elevational gradients of species distributions. Additionally, we model that the presence of vegetation improves soil permeability based on Eq. 7. This allows us to simulate plant species cooperation: less precipitation-adapted species serve as pioneers for improving soil permeability, which consequently becomes a preferential habitat for a more precipitation-adapted species. Geomorphic controls on vegetation composition and plant species cooperation are well documented in scientific literature [Bertuzzo et al. 2016; Bonan 2015].

In Fig. 15 we show the results of an ablation study of the impact of the soil model with enabled and disabled microclimate. We compare two identical developing ecosystems that are comprised of two plant species. The yellow plant species is more precipitation-adapted than the green species. After a few iterations, in both microclimate-enabled (top) and microclimate-disabled (bottom) simulations the distribution of yellow and green species is similar (a, e). However,

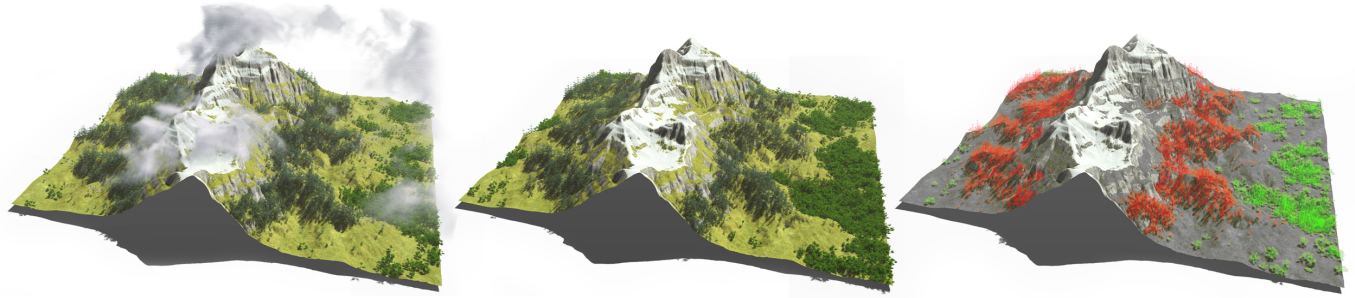

Fig. 18. Our method is able to capture complex wind-vegetation interactions (left). One example is the Foehn effect which causes a temperature gradient over a mountain slope. The change of temperatures in the microclimate leads to different compositions of vegetation on the leeward and windward side of the mountain (center). Different species are highlighted with different color (right).

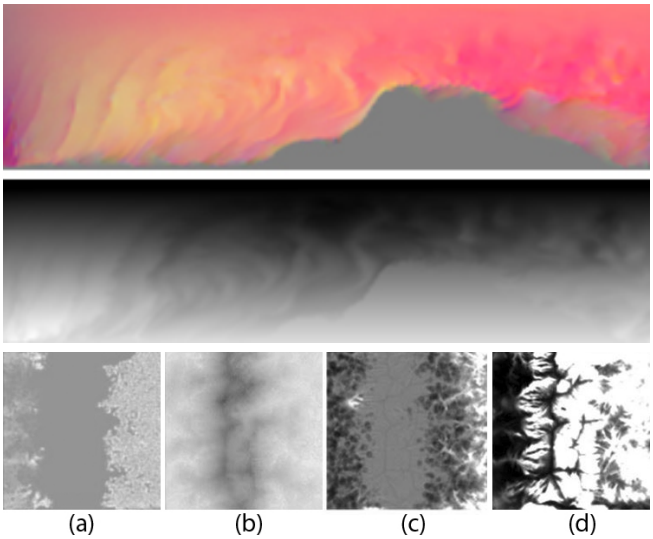

Fig. 19. Top and middle row: side view of velocity (top) and temperature (middle) profiles illustrating the Foehn effect discussed in Fig. 18. Due to the interaction of the wind field with the mountain side a differential temperature gradient results. The left side of the mountain is cooler than the right side (velocity field rendered as RGB colors). The color image indicating velocities shows turbulence on the right side of the mountain. Bottom row: top-down views of the vapor, temperature, soil and precipitation maps, respectively. The vapor map indicates the less pronounced vegetation presence on the left side of the mountain (a), cooler temperatures at higher elevation (b), wetter soil on the right side (c) and the regions of high precipitation (d). For all maps brighter colors indicate higher values.

after further development an elevational gradient for the green species is emerging in the microclimate-enabled case (b, c), whereas the microclimate-disabled simulation exhibits uniform growth (f, g). After soil permeability has been increased by the green species, the more precipitation-adapted yellow species appears in the crevasses of the terrain for the microclimate-enabled case (d) – an example of species cooperation. The microclimate-disabled simulation does not capture this succession of species (h). This result demonstrates that our model effectively captures emergently plant species successions by simulating competition as well as cooperation.

7.2.2 Edge Effects. It has been recognized that human-caused forest fragmentation leads to increased edge effects, e.g. in the South American rainforest [Broadbent et al. 2008]. Edges of forests are known to exhibit steep climatic gradients which lead to different vegetation distribution, species richness, and vegetation growth attributes.

Our microlimate models allows us to emergently simulate edge effects. In Fig.17 we show the results of an developing ecosystem composed of four different plant species. Three smaller species are more drought-adapted compared to a taller climax species. Initially, we start with a mixed stand of plants (a). Over time, the locally varying microclimate leads to drier regions at the forest edge and a wetter region inside the forest. This causes the drought-adapted species to preferentially grow at the edges of the forest, while the climax species favors the wetter interior (b). To show the emergence of edge effects we removed all tree models near the center line of the forest patch (c). The regrowing forest patch exhibits similar edge effects as before, where drought-adapted species develop near the center line (d). This phenomenon is completely dependent on a local specification of the climate and cannot be obtained by non-local ecoclimate models.

7.2.3 Deforestation Effects. Simulating vegetation in a detailed and individual-based way also allows us to express a local vegetation-atmosphere feedback. We demonstrate this in Fig. 16 where we show an extreme case of this feedback to cloud formation. By keeping the macroclimatic parameter values constant during the simulation we ensure consistent cloud formation patterning over a dense rainforest landscape (a). Then, we remove a large patch of the rainforest, which results in drastic changes to the values stored in the vapor map. As a result, vapor values in the *Weather Voxel Space* above the deforested area drop below the cloud formation threshold (b). Finally, we continue vegetation growth for several years until clouds are again observable above the previously deforested region (c, d). In our simulation, each plant of the vegetation model contributes through evaporation to the hydrological cycle leading to local variations of the atmosphere. This local feedback is a novel topic of climate research and referred to as surface heterogeneity control of cloud formation [Xiao et al. 2018].

7.2.4 Foehn Effects. As another example for the importance of the microclimate we simulate the Foehn effect – a phenomenon that requires a local atmosphere-vegetation feedback instead of a purely global one. The Foehn effect is characterized by a temperature gradient resulting from a laminar wind flow over a steep mountain

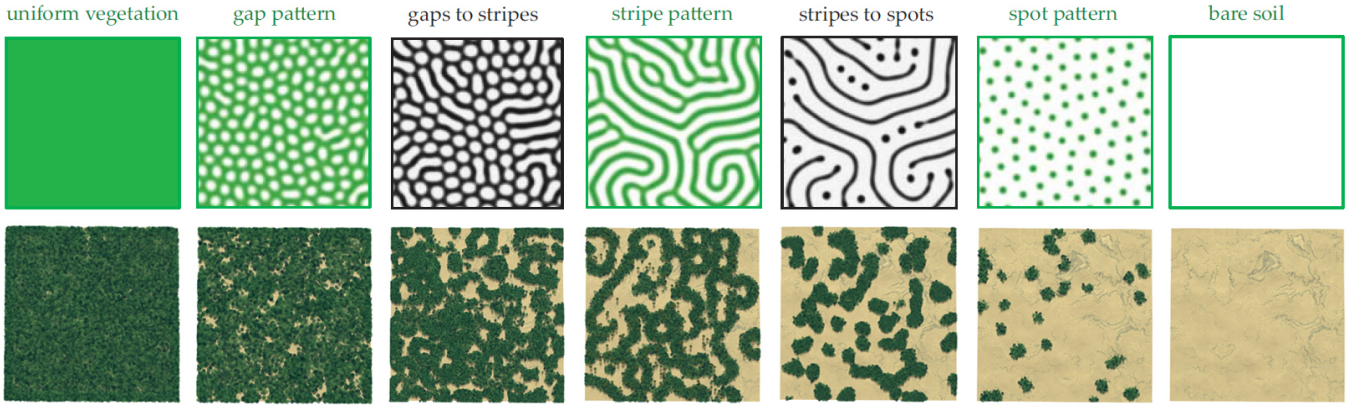

Fig. 20. Our results correspond to the recent analytical study performed in ecology research (top row, adapted from [Meron 2019], Fig. 5) which highlights morphological transitions (black and white panels) between gap, stripe and spot patterns (green panels). Our method simulates similar spatial vegetation patterns obtained by different the macroscopic vapor E_M (values decreasing from left to right).

ridge. This atmospheric change may impact vegetation development resulting in differential ecosystem compositions on either side of the mountain. This complex effect is captured in an emergent way by our method (Fig. 18, left). Due to the non-uniform boundary conditions imposed by a mountainous height map the uniform, unidirectional wind field is oriented upwards in our simulation grid, which results in a cooling of air. Fig. 19 shows the resulting velocity (top) and temperature (bottom) profiles. On the other side of the mountain the down-flowing air heats up again and exhibits turbulent air motion. This results in a warmer leeward mountain side (center), which is indicated by the lighter colors in the temperature profile. In this scene, we placed two species with varying temperature adaptation and simulated their growth for 200 years. For the resulting ecosystem we can observe that the forest on the windward side is composed of only the cold-adapted conifers. Whereas, on the other side both plant species establish themselves. The species distribution is illustrated in Fig. 18 (right) by color-coding the two plant species of the ecosystem (red denotes the cold-adapted conifers, green the warm-adapted deciduous trees). Please note that for this experiment we do not consider the geographic orientation of the scene, e.g. the light exposure differences between north and south facing slopes.

7.3 Comparative Analysis

To evaluate the plausibility of our simulations we conduct a series of comparative analyses to theoretical studies in climatology and ecology research, as well as to real world examples.

In Fig. 20 we show a comparison of our simulated results to Meron [2019], an analytical study of the formation of spot and stripe patterns. Meron [2019] describes the response of vegetation to various precipitation regimes. Specifically, they propose a vegetation growth model which only depends on the impact of precipitation. Further, their method expresses vegetation abstractly as concentrations of biomass. In contrast, our method considers also light, temperature and represents vegetation geometrically. This way our method allows us to express non-trivial feedback loops for competition for water and light, as well as cooperation for improving water infiltration (Eqs. 6 and 7). This allows us to express Turing-like

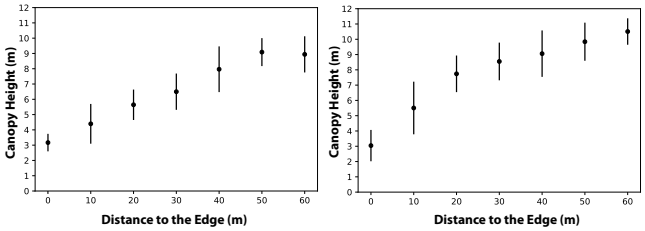

Fig. 21. Canopy height depicted as a function of distance to the forest edge (canopy > 1 meter) for a mixed forest (left) and a pine forest (right). These canopy profiles conform with observations reported for forests in a subtropical climate [Delgado et al. 2007]: the pine forest has a steeper gradient of canopy height compared to the mixed forest.

patterns via short-distance inhibition due to plants competing for the same space and long-distance promotion of plant development due to improving soil permeability. We explore the capability of our method and compare to the results reported by Meron [2019] describing a variety of spot, gap, and stripe patterns, as well as their morphological transitions (Fig. 20, top). Analogously, to their method we can express all these spatial vegetation patterns as a function of the vapor parameter E_M (Fig. 20, bottom). These patterns can be simulated in a steady state over longer periods of simulation time, i.e. we simulated an ecosystem for 500 years and observed no qualitative change for specific patterns. Additionally, our soil model considers the topography and therefore also captures the feedback between terrain slopes and spatial vegetation patterning (Fig. 24). Corresponding average plots of surface and soil water are included in the appendix for reference (Fig. 25). These results indicate that our method is realistically modeling the precipitation response of vegetation.

Time scales of forest growth make experimental research studies on ecoclimates inherently difficult to conduct. Therefore, ecologists commonly employ analytical approaches. Recent theoretical results indicate that vegetation response to climate change can vary according to the rate of change of climatic conditions. For example, [Bastiaansen et al. 2020; Rietkerk et al. 1997] conducted theoretical experiments to study the differential response of vegetation to varying speeds of climate change by reducing the rate of precipitation by

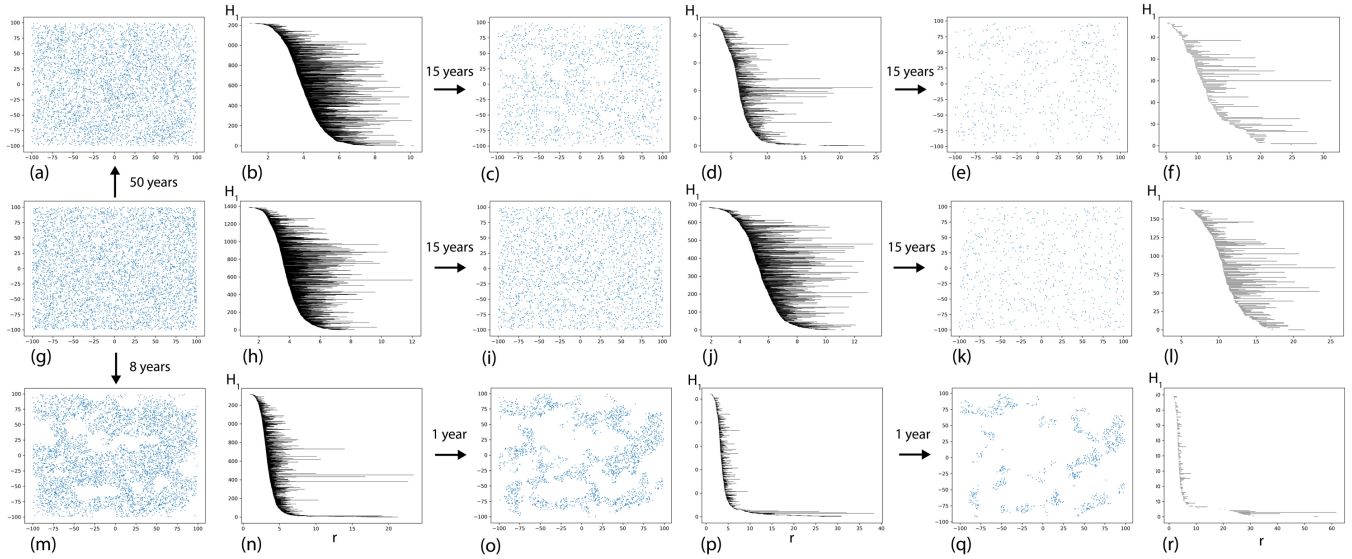

Fig. 22. We evaluate the impact of three climate change simulations on the same initial vegetation pattern composed of a single plant species. We show plant distributions as scatter plots with blue points indicating plant positions on the ground surface and the corresponding H_1 persistent homology barcodes obtained from the point clouds. The initial vegetation scene before decreasing vapor values is depicted in (g), and its barcode is shown in (h). The results of a naive ecoclimate model without microclimates is shown in (i-l) - no persistent topological features emerge. In the top row (a-f), we show plant distributions and barcodes for a slow climate change scenario with microclimates. In this case, more persistent topological features emerge. In the bottom row (m-r), we show plant distributions and barcodes for a fast climate change scenario (10 times faster vapor value decrease than the slow scenario) with microclimates. Here, the barcodes reveal that topological features are more persistent than in the other scenarios. The plant distribution appears less uniformly spread across space compared to both the naive, as well as the slow climate change model.

a factor of 10. In their slow climate change experiment they observe that spatial patterning of vegetation corresponds to a more uniform distribution compared to the fast climate change experiment. This discrepancy is explained by the additional time that plants have to redistribute across space and more efficiently take up soil water. Furthermore, the interconnection between climate and vegetation has been described as a tipping point phenomenon [Rietkerk et al. 2004]. According to these findings vegetation response to climate change may be unnoticeable for long periods of time and then unexpectedly shift catastrophically.

Similar to these studies, we conducted experiments to evaluate whether our method also captures (1) varying vegetation response to slow and fast climate change; and (2) the occurrence of tipping points and catastrophic shifts. The results are shown in Fig. 22. Our goal is to compare a slow (a-f) and a fast (m-r) climate change scenario by changing vapor E_M with different rates (10 times difference) over time. Additionally, we compare both scenarios with a baseline that does not use microclimates (h-l). The initial ecosystem used for all scenarios is shown in (g). Plant distributions are shown as scatter plots with blue points. To quantitatively assess the progression of the three ecosystems we use persistent homology to measure the topological features of plant distributions, such as spots, gaps, and stripes. To illustrate the changes of vegetation patterning over time we assess the persistence of topological features as H_1 barcodes for each plant distribution. Long barcodes indicate persisting topological features whereas short barcodes indicate noise.

Starting with an initial ecosystem the result of a climate change scenario without microclimates is shown in (g-l). As shown in the scatter plots (g, i, k), the plant distributions for this simulation remain randomly distributed, while the overall number of plants diminishes. The barcodes (h, j, l) do not contain persistent topological features indicating a lack of catastrophic shifts of vegetation patterning.

The fast climate change scenario is shown in the plots (m-r). Starting from the initial plant distribution (g) we simulate climate change over a period of 10 years. In contrast to the baseline without microclimates, the scatter plots illustrate clustered distributions of plants (m, o, q). Moreover, the corresponding barcodes (n, p, r) expose the presence of persisting topological features indicating the presence of gaps in the plant distributions. These features appear over a short period of time (p, r) thereby indicating a tipping point phenomenon.

Finally, the slow climate change scenario is shown in the plots (a-f). For this scenario climate changes takes place over a period of 80 years. The distribution of plants initially changes less significantly, but then also hits a tipping point after 64 years (c) that consequently results in a severely reduced plant distribution (f). The changes of plant distributions and topological features for this scenario can be observed in (b, d, f).

These climate change scenarios illustrate that our method realistically captures the formation and expansion of forest gaps resulting from catastrophic shifts. In addition, our method produces more dispersed plant distributions for the slow climate change scenario which corresponds to research results reported in ecology [Bastiaansen et al. 2020; Rietkerk et al. 2004]. The model without microclimates does not capture these phenomena and thus does not simulate climate change in a plausible way.

We further evaluate our model by quantitatively assessing canopy height distributions. We simulate two forest patches, one composed of a mixed stand of different plant species, and a forest composed only of pine trees. The results of this experiment are reported in Fig. 21. Canopy height gradients at the forest edge are steeper for the pine forest (right) compared to the mixed tree stand (left) as a result of differential microclimates. This qualitatively conforms to observations in the subtropical region reported by Delgado et al. [2007].

Our method enables the exploration of a vast array of different ecoclimatic phenomena, which can be validated with comparisons to real world observations. In Fig. 23 we show qualitative comparisons of our simulation results to real photographs. In particular, we show a comparison of an arid ecosystem in Niger (a, b) and a comparison to peatlands in Western Siberia (c, d). As illustrated our method enables simulating ecoclimates with high visual similarity of spatial vegetation patterning compared to real ecosystems. Photographs were taken from [Rietkerk et al. 2004].

8 DISCUSSION AND LIMITATIONS

We have presented a method for simulating ecoclimates capable of generating highly realistic images. At the core of our method lies the modeling of a detailed, bidirectional feedback between clouds and vegetation that captures phenomena such as spatial patterning in ecosystems, varied vegetation gradients on forest edges, realistic features in different climate change scenarios, and plausible dynamics of cloud formation over different biomes. In contrast to methods that are based on authoring clouds or ecosystems our approach relies on a mechanistic description of the various biological and physical processes. This allows our method to generate not only momentary views of the cloud- and ecosystem-related phenomena but also to express their emergent dynamics over different time scales. However, these advantages are balanced by a generally slower run-time compared to a more descriptive, authoring approach.

Furthermore, we extend existing simulation work in graphics by demonstrating how stable patterning of vegetation can be obtained. In previous methods [Makowski et al. 2019] spatial vegetation patterns are only modeled transiently and not to the same degree of realism. Our method improves cloud dynamics by incorporating heat transfer and vapor released by vegetation resulting in more realistic cloud distribution. Moreover, the joint simulation of ecosystem, soil and cloud models allows emergently capturing phenomena, such as the Foehn effect. However, we do not take into account the complex hydrological dynamics between water bodies, soil and vegetation, which limits the scope of cloud formation phenomena that can be modeled.

Compared to analytical models studied in ecology research, our method expresses plant growth and their spatial interaction with considerably greater realism by describing detailed 3D geometry of plants and their microclimate. We aid research in ecology by demonstrating that realistic spatial patterning of vegetation can be explained by a model relying on plant competition for light as well as their cooperation for soil permeability, rather than competition for water uptake alone. Furthermore, we show that emerging microclimates due to weather and vegetation feedback are sufficient to qualitatively explain forest edge effects. These findings indicate that our model may serve as a theoretical framework for testing ecological research hypotheses in the future.

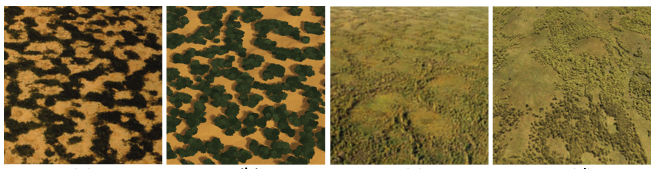

Fig. 23. Comparison of a photograph of an arid ecosystem in Niger (a) and our simulation result (b), as well as a photograph of peatlands in Western Siberia (c) and our corresponding simulation (d). Our method is able to generate realistic spatial vegetation patterns for different environments. Photographs are taken with permission from Rietkerk et al. [2004].

In climate research, large eddy simulations are used to study ecoclimates with similar spatial fidelity compared to our method. These approaches generally describe the water transfer between vegetation and atmosphere using some variation of the Penman-Monteith (PM) equation. These types of models rely on a spatially averaged description of vegetation and consequently do not allow for the realistic rendering of individual plant geometry. In our method, plants are treated in an individual-based way meaning that vegetation-atmosphere feedback is described at a lower scale of abstraction compared to PM models. This allows to formulate and test hypotheses which rely on such detailed representation. In general, state-of-the-art climate models describe and study feedbacks which we did not take into account, e.g. the diurnal cycle, variations of directional lighting caused by seasonal changes, or light-mediated feedback between terrain and the atmosphere (i.e. solar irradiance). Specifically, adding the geographic orientation and the resulting shading differences of sloped terrain would make a reconstruction of ecoclimates in mountainous scenes more realistic. For example, in hilly terrain physically plausible modeling of irradiance would lead to more realistic cloud formation compared to our simplified approach. On the other hand, our results indicate that for the phenomena simulated in this work a detailed model of irradiance is not required. However, adding such advanced physical processes could lead to higher predictive qualities of our model.

9 CONCLUSION

In this paper, we have advanced 3D outdoor scene modeling by introducing a method that for the first time captures realistic vegetation development in response to climate change. Our method is based on the coupling of complex models of plant ecosystems, soil hydrology, and weather. This enables us to express important feedback loops between the different climate systems to simulate ecoclimates with an unprecedented degree of detail. We have presented a variety of patterns that can be explored with a coupled vegetation, soil and weather model. These patterns are controlled by mechanisms occurring at different time scales - from seconds to years. This poses considerable modelling challenges which we addressed here by leveraging state-of-the-art models for cloud formation, vegetation modeling and recent advances in climate research. Although complex in construction, by a lightweight interface our method allows for the interactive exploration of a parameter space containing

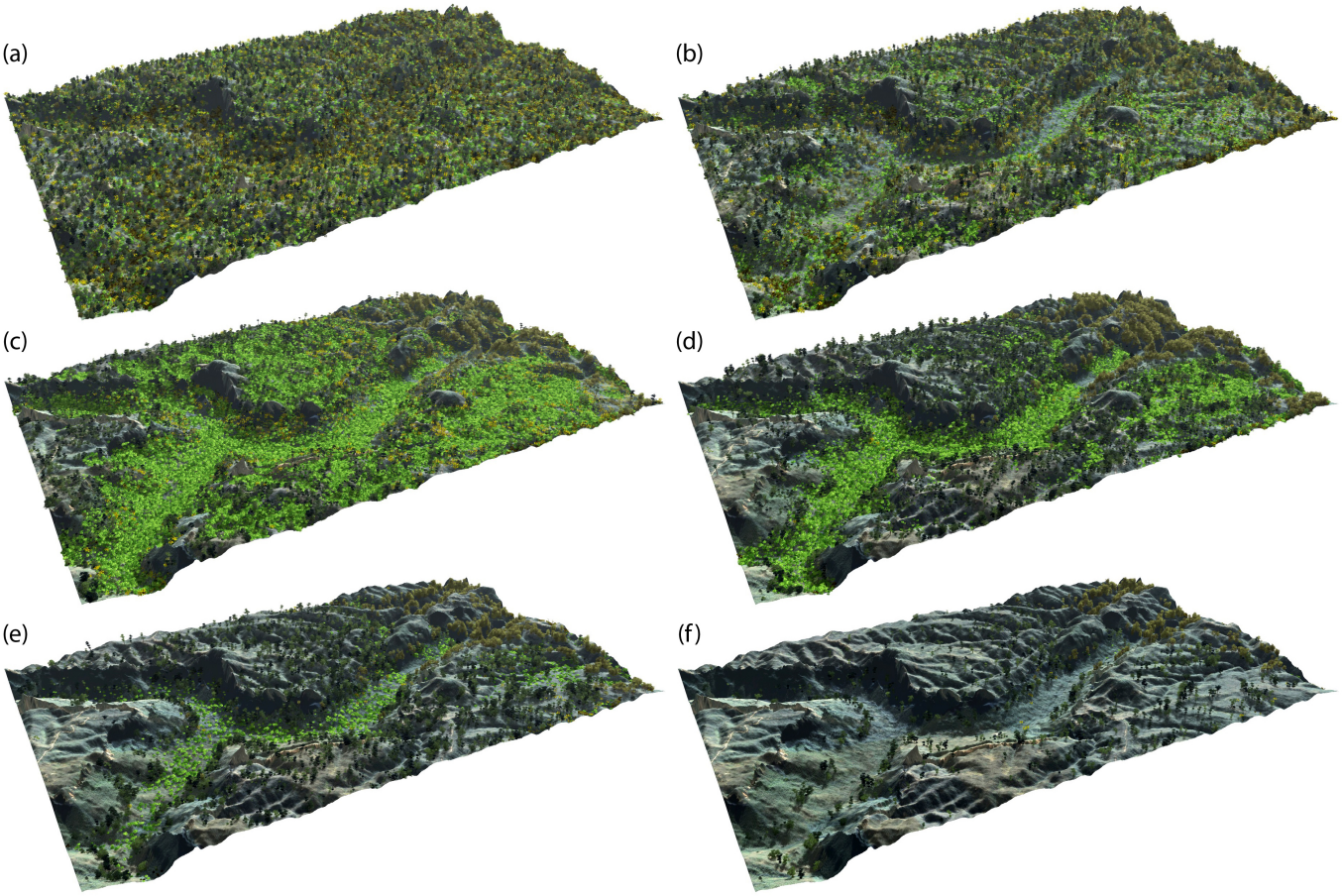

Fig. 24. In this result we demonstrate the visual complexity of ecosystems in relation to climate dynamics. A tropical forest scene with 4300mm average annual precipitation contains six mixed species uniformly distributed across the terrain (a). As precipitation decreases to 3700mm the less well-adapted tree species die back forming large forest gaps (b). This allows fast growing and more climate-adapted species to proliferate, changing the forest composition in the process (c, 2500mm). As the climate further changes plant species segregate to exploit climatic niches on the terrain (d, 1260mm). Finally, continued precipitation decrease results in arid vegetation pattern (e-f, 900-400mm). Our shadow propagation algorithm allows for local variations of light exposure at the sloped regions of the terrain, global light variations are not considered.

phenomena which have never been described before in computer graphics. These include detailed descriptions of self-organized spatial patterning in arid ecosystems, varied vegetation gradients on forest edges, realistic features in different climate change scenarios, and feedback of vegetation on cloud formation dynamics.

The current state of our framework opens several avenues for future work. For one, it seems interesting to extend our method for testing ecoclimate hypotheses and validating these findings with other analytical and empirical observations. Second, it seems possible to further increase the realism of our model, for example by introducing the diurnal cycle to describe variations of temperature during night and day, or by taking local irradiance patterns into account. Additionally, it seems interesting to combine our method with models of the pedosphere and cryosphere. Finally, we want to further develop our model for exploring the adaptation of vegetation to climate change as recent ecology research indicates that microclimates may have a significant impact on ecosystem development. Here our detailed geometric plant representation can aid research in ecology because current models for climate change do not focus on modeling microclimates. All these research directions could advance our method towards a more universal simulation of ecoclimate dynamics.

ACKNOWLEDGMENTS

We thank the reviewers for their valuable comments that help to improve the manuscript.

REFERENCES

R. P. Allan, M. Barlow, M. P. Byrne, A. Cherchi, H. Douville, H. J. Fowler, T. Y. Gan, A. G. Pendergrass, D. Rosenfeld, A. L. S. Swann, L. J. Wilcox, and O. Zolina. 2020. Advances in understanding large-scale responses of the water cycle to climate change. *Ann. N.Y. Acad. Sci.* (2020).

M. Aono and T.L. Kunii. 1984. Botanical Tree Image Generation. *IEEE Comput. Graph. Appl.* 4(5) (1984), 10–34.

O. Argudo, C. Andújar, A. Chica, E. Guérin, J. Digne, A. Peytavie, and E. Galin. 2017. Coherent multi-layer landscape synthesis. *The Visual Computer* 33, 6 (2017), 1005–1015.

R. Bastiaansen, A. Doelman, M. B. Eppinga, and M. Rietkerk. 2020. The effect of climate change on the resilience of ecosystems with adaptive spatial pattern formation. *Ecology Letters* 23, 3 (2020), 414–429.

B. Beneš, N. Andrysco, and O. Šťava. 2009. Interactive Modeling of Virtual Ecosystems. In *Proceedings of the Fifth Eurographics Conference on Natural Phenomena (NPH'09)*. Eurographics Association, Goslar, DEU, 9–16.

E. Bertuzzo, F. Carrara, L. Mari, F. Altermatt, I. Rodriguez-Iturbe, and A. Rinaldo. 2016. Geomorphic controls on elevational gradients of species richness. 113, 7 (2016), 1737–1742.

G. Bonan. 2015. *Ecological Climatology: Concepts and Applications* (3 ed.). Cambridge University Press.

A. Bouthors, F. Neyret, N. Max, E. Bruneton, and C. Crassin. 2008. Interactive Multiple Anisotropic Scattering in Clouds. In *I3D (2008)*. 173–182.

D. Bradley, D. Nowrouzezahrai, and P. Beardsley. 2013. Image-based Reconstruction Synthesis of Dense Foliage. *ACM Trans. Graph.* 32, 4, Article 74 (2013), 74:1–74:10 pages.

E. N. Broadbent, G. P. Asner, M. Keller, D. E. Knapp, P. J. C. Oliveira, and J. N. Silva. 2008. Forest fragmentation and edge effects from deforestation and selective logging in the Brazilian Amazon. *Biological Conservation* 141, 7 (2008), 1745 – 1757.

E. Bruneton and F. Neyret. 2012. Real–time Realistic Rendering and Lighting of Forests. *Comput. Graph. Forum* 31, 2pt1 (2012), 373–382.

E. Ch'ng. 2011. Realistic Placement of Plants for Virtual Environments. *IEEE Comput. Graph. Appl.* 31, 4 (2011), 66–77.

G. Cordonnier, E. Galin, J. Gain, B. Benes, E. Guérin, A. Peytavie, and M.-P. Cani. 2017. Authoring Landscapes by Combining Ecosystem and Terrain Erosion Simulation. *ACM Trans. Graph.* 36, 4, Article 134 (2017), 12 pages.

J. Delgado, N. Arroyo, J. R. Arevalo, and J. Fernández-Palacios. 2007. Edge effects of roads on temperature, light, canopy cover, and canopy height in laurel and pine forests (Tenerife, Canary Islands). *Landscape and Urban Planning* (07 2007), 328–340.

O. Deussen, C. Colditz, M. Stamminger, and G. Drettakis. 2002. Interactive Visualization of Complex Plant Ecosystems. *VIS '02* (2002), 219–226.

O. Deussen, P. Hanrahan, B. Lintermann, R. Měch, M. Pharr, and Przemyslaw Prusinkiewicz. 1998. Realistic Modeling and Rendering of Plant Ecosystems. *ACM Trans. Graph.* (1998), 275–286.

P. Ecormier-Nocca, G. Cordonnier, P. Carrez, A.-M. Moigne, P. Memari, B. Benes, and M.-P. Cani. 2021. Authoring Consistent Landscapes with Flora and Fauna. *ACM Trans. Graph.* 40, 4, Article 105 (2021), 13 pages.

C. W. Ferreira Barbosa, Y. Dobashi, and T. Yamamoto. 2015. Adaptive Cloud Simulation Using Position Based Fluids. *Comput. Animat. Virtual Worlds* 26, 3–4 (2015), 367–375.

J. Gain, H. Long, G. Cordonnier, and M.-P. Cani. 2017. EcoBrush: Interactive Control of Visually Consistent Large-Scale Ecosystems. *Computer Graphics Forum* 36, 2 (2017), 63–73.

P. Goswami and F. Neyret. 2017. Real-Time Landscape-Size Convective Clouds Simulation and Rendering. In *Proceedings of the 13th Workshop on Virtual Reality Interactions and Physical Simulations (VRIPHYS '17)*. Eurographics Association, 1–8.

T. Hädrich, D. T. Banuti, W. Pałubicki, S. Pirk, and D. L. Michels. 2021. Fire in Paradise: Mesoscale Simulation of Wildfires. *ACM Trans. Graph.* 40, 4, Article 163 (2021).

T. Hädrich, B. Benes, O. Deussen, and S. Pirk. 2017. Interactive Modeling and Authoring of Climbing Plants. *CGF* 36, 2 (2017), 49–61.

T. Hädrich, M. Makowski, W. Pałubicki, D. Banuti, S. Pirk, and D. L. Michels. 2020. Stormscapes: Simulating Cloud Dynamics in the Now. *ACM Transactions on Graphics (Proceedings of SIGGRAPH Asia)* (2020).

M. J. Harris, W. V. Baxter, T. Scheuermann, and A. Lastra. 2003. Simulation of Cloud Dynamics on Graphics Hardware. In *ACM SIGGRAPH/EUROGRAPHICS Conference on Graphics Hardware (HWWS '03)*. Eurographics Association, 92–101.

J. A. A. Herrera, T. Hädrich, W. Pałubicki, D. T. Banuti, S. Pirk, and D. L. Michels. 2021. Weatherscapes: Nowcasting Heat Transfer and Water Continuity. *ACM Trans. Graph.* 40, 6, Article 204 (2021), 19 pages.

R. HilleRisLambers, M. Rietkerk, F. van den Bosch, H. H. T. Prins, and H. de Kroon. 2001. Vegetation Pattern Formation in Semi-Arid Grazing Systems. *Ecology* 82, 1 (2001), 50–61.

G. L. Horn, H. G. Ouwersloot, J. Vilà-Guerau de Arellano, and M. Sikma. 2015. Cloud Shading Effects on Characteristic Boundary-Layer Length Scales. *Boundary-Layer Meteorology* 157, 2 (01 Nov 2015), 237–263.

T. Ijiri, S. Owada, and T. Igarashi. 2006. Seamless Integration of Initial Sketching and Subsequent Detail Editing in Flower Modeling. *Comp. Graph. Forum* 25, 3 (2006), 617–624.

M. Jaeger and J. Teng. 2003. Tree and plant volume imaging - An introductive study towards voxelized functional landscapes. *PMA* (2003).

K. Kapp, J. Gain, E. Guérin, E. Galin, and A. Peytavie. 2020. Data-driven Authoring of Large-scale Ecosystems. *ACM Trans. Graph.* (2020).

E. Kessler. 1969. *On the Distribution and Continuity of Water Substance in Atmospheric Circulations.* American Meteorological Society, Boston, MA, 1–84.

M. Kovenock and A. L. S. Swann. 2018. Leaf Trait Acclimation Amplifies Simulated Climate Warming in Response to Elevated Carbon Dioxide. *Global Biogeochemical Cycles* 32, 10 (2018), 1437–1448.

P. K. Kundu, I. M. Cohen, and D. R. Dowling. 2012. *Fluid Mechanics.* Elsevier Science.

B. Lane and P. Prusinkiewicz. 2002. Generating Spatial Distributions for Multilevel Models of Plant Communities. *Graphics Interface* (2002), 69–80.

B. Li, J. Kałużny, J. Klein, D. L. Michels, W. Pałubicki, B. Benes, and S. Pirk. 2021. Learning to Reconstruct Botanical Trees from Single Images. *ACM Transaction on Graphics* 40, 6, Article 231 (12 2021).

C. Li, O. Deussen, Y.-Z. Song, P. Willis, and P. Hall. 2011. Modeling and Generating Moving Trees from Video. *ACM Trans. Graph.* 30, 6, Article 127 (2011), 127:1–127:12 pages.

P. Liang, X. Wang, H. Sun, Y. Fan, Y. Wu, X. Lin, and J. Chang. 2019. Forest type and height are important in shaping the altitudinal change of radial growth response to climate change. *Scientific Reports* 9, 1 (2019), 1336.

B. Lintermann and O. Deussen. 1999. Interactive Modeling of Plants. *IEEE Comput. Graph. Appl.* 19, 1 (Jan. 1999), 56–65. https://doi.org/10.1109/38.736469

Y. Livny, S. Pirk, Z. Cheng, F. Yan, O. Deussen, D. Cohen-Or, and B. Chen. 2011. Texture-lobes for Tree Modelling. *ACM Trans. Graph.* 30, 4, Article 53 (2011), 10 pages.

S. Longay, A. Runions, F. Boudon, and P. Prusinkiewicz. 2012. TreeSketch: interactive procedural modeling of trees on a tablet. In *Proc. of the Intl. Symp. on SBIM*. 107–120.

M. Makowski, T. Hädrich, J. Scheffczyk, D. L. Michels, S. Pirk, and W. Pałubicki. 2019. Synthetic Silviculture: Multi-Scale Modeling of Plant Ecosystems. *ACM Trans. Graph.* 38, 4, Article 131 (2019), 14 pages.

N. Maréchal, E. Guérin, E. Galin, S. Mérillou, and N. Mérillou. 2010. Heat Transfer Simulation for Modeling Realistic Winter Sceneries. *CGF* 29 (05 2010), 449 – 458.

E. Meron. 2019. Vegetation pattern formation: The mechanisms behind the forms. *Physics Today* 72, 11 (2019), 30–36.

R. Miyazaki, S. Yoshida, T. Nishita, and Y. Dobashi. 2001. A Method for Modeling Clouds Based on Atmospheric Fluid Dynamics. In *PG*. IEEE Computer Society, USA, 363.

R. Měch and P. Prusinkiewicz. 1996. Visual models of plants interacting with their environment. In *Proc. of SIGGRAPH*. ACM, 397–410.

B. Neubert, T. Franken, and O. Deussen. 2007. Approximate Image-based Tree-modeling Using Particle Flows. *ACM Trans. Graph.* 26, 3, Article 88 (2007).

B. Neubert, S. Pirk, O. Deussen, and C. Dachsbacher. 2011. Improved Model- and View-Dependent Pruning of Large Botanical Scenes. *Comp. Graph. Forum* 30, 6 (2011), 1708–1718.

F. Neyret. 1997. Qualitative Simulation of Convective Cloud Formation and Evolution. In *Computer Animation and Simulation '97*, D. Thalmann and M. van de Panne (Eds.). Springer Vienna, Vienna, 113–124.

T. Niese, S. Pirk, M. Albrecht, B. Benes, and O. Deussen. 2022. Procedural Urban Forestry. *ACM Transaction on Graphics* 41, 1 ((in press) 2022).

M. Okabe, S. Owada, and T. Igarashi. 2007. Interactive Design of Botanical Trees Using Freehand Sketches and Example-based Editing. In *ACM SIGGRAPH Courses*. ACM, Article 26.

P. E. Oppenheimer. 1986. Real time design and animation of fractal plants and trees. *Proc. of SIGGRAPH* 20, 4 (1986), 55–64.

D. Overby, Z. Melek, and J. Keyser. 2002. Interactive physically-based cloud simulation. In *10th Pacific Conference on Computer Graphics and Applications, 2002. Proceedings.* 469–470.

W. Palubicki, K. Horel, S. Longay, A. Runions, B. Lane, R. Měch, and P. Prusinkiewicz. 2009. Self-organizing Tree Models for Image Synthesis. *ACM Trans. Graph.* 28, 3, Article 58 (2009), 10 pages.

S. Pirk, B. Benes, T. Ijiri, Y. Li, O. Deussen, B. Chen, and R. Měch. 2016. Modeling Plant Life in Computer Graphics. In *ACM SIGGRAPH 2016 Courses*. ACM, Article 18, 180 pages.

S. Pirk, M. Jarząbek, T. Hädrich, D. L. Michels, and W. Palubicki. 2017. Interactive Wood Combustion for Botanical Tree Models. *ACM Trans. Graph.* 36, 6, Article 197 (2017), 12 pages.

S. Pirk, T. Niese, T. Hädrich, B. Benes, and O. Deussen. 2014. Windy Trees: Computing Stress Response for Developmental Tree Models. *ACM Trans. Graph.* 33, 6, Article 204 (2014), 11 pages.

S. Pirk, O. Stava, J. Kratt, M. A. M. Said, B. Neubert, R. Měch, B. Benes, and O. Deussen. 2012. Plastic trees: interactive self-adapting botanical tree models. *ACM Trans. Graph.* 31, 4, Article 50 (2012), 10 pages.

H. Pretzsch, R. Grote, B. Reineking, T. Rötzer, and S. Seifert. 2008. Models for Forest Ecosystem Management: A European Perspective. *Annals of botany* 101 (06 2008), 1065–87.

R. M. Pringle and C. E. Tarnita. 2017. Spatial Self-Organization of Ecosystems: Integrating Multiple Mechanisms of Regular-Pattern Formation. *Annual Review of Entomology* 62, 1 (2017), 359–377.

P. Prusinkiewicz. 1986. Graphical applications of L-systems. In *Proc. on Graph. Interf.* 247–253.

L. Quan, P. Tan, G. Zeng, L. Yuan, J. Wang, and S. B. Kang. 2006. Image-Based Plant Modeling. *ACM Trans. Graph.* 25, 3 (2006), 599–604.

M. Rietkerk, S. C. Dekker, P. C. de Ruiter, and J. van de Koppel. 2004. Self-Organized Patchiness and Catastrophic Shifts in Ecosystems. *Science* 305, 5692 (2004), 1926–1929.

M. Rietkerk, F. van den Bosch, and J. van de Koppel. 1997. Site-Specific Properties and Irreversible Vegetation Changes in Semi-Arid Grazing Systems. *Oikos* 80, 2 (1997), 241–252.

L. Ringham, A. Owens, M. Cieslak, L. D. Harder, and P. Prusinkiewicz. 2021. Modeling Flower Pigmentation Patterns. *ACM Trans. Graph.* 40, 6, Article 233 (2021), 14 pages.
H. Shao, T. Kugelstadt, T. Hädrich, W. Pałubicki, J. Bender, S. Pirk, and Dominik L. Michels. 2021. Accurately Solving Rod Dynamics with Graph Learning. In *NeurIPS*.
J. Stam. 1999. Stable Fluids. *Proc. of ACM SIGGRAPH* (1999), 121–128.
O. Stava, S. Pirk, J. Kratt, B. Chen, R. Měch, O. Deussen, and B. Benes. 2014. Inverse Procedural Modelling of Trees. *CGF* 33, 6 (2014), 118–131.
P. Tan, T. Fang, J. Xiao, P. Zhao, and L. Quan. 2008. Single Image Tree Modeling. *ACM Trans. Graph.* 27, 5, Article 108 (2008), 7 pages.
U. Vimont, J. Gain, M. Lastic, G. Cordonnier, B. Abiodun, and M.-C. Cani. 2020. Interactive Meso-scale Simulation of Skyscapes. *Eurographics* (2020).
H. Y. Wang, M. Z. Kang, J. Hua, and X. J. Wang. 2013. Modeling Plant Plasticity from a Biophysical Model: Biomechanics. In *Proceedings of the 12th ACM SIGGRAPH Intl. Conf. on VRCAI*. ACM, 115–122.
A. Webanck, Y. Cortial, E. Guérin, and E. Galin. 2018. Procedural Cloudscapes. *CGF* 37, 2 (2018), 431–442.
J. Wither, F. Boudon, M.-P. Cani, and C. Godin. 2009. Structure from silhouettes: a new paradigm for fast sketch-based design of trees. *CGF* 28, 2 (2009), 541–550.
H. Xiao, L. K. Berg, and M. Huang. 2018. The Impact of Surface Heterogeneities and Land-Atmosphere Interactions on Shallow Clouds Over ARM SGP Site. *Journal of Advances in Modeling Earth Systems* 10, 6 (2018), 1220–1244.
H. Xu, N. Gossett, and B. Chen. 2007. Knowledge and heuristic-based modeling of laser-scanned trees. 26, 4 (2007), Article 19, 13 pages.
F. Zellweger, P. De Frenne, J. Lenoir, P. Vangansbeke, K. Verheyen, M. Bernhardt-Römermann, L. Baeten, R. Hédl, I. Berki, J. Brunet, H. Van Calster, M. Chudomelová, G. Decocq, T. Dirnböck, T. Durak, T. Heinken, B. Jaroszewicz, M. Kopecký, F. Máliš, M. Macek, M. Malicki, T. Naaf, T. A. Nagel, A. Ortmann-Ajkai, P. Petřík, R. Pielech, K. Reczyńska, W. Schmidt, T. Standovár, K. Świerkosz, B. Teleki, O. Vild, M. Wulf, and D. Coomes. 2020. Forest microclimate dynamics drive plant responses to warming. *Science* 368, 6492 (2020), 772–775.
B. Zhang and D. L. DeAngelis. 2020. An overview of agent-based models in plant biology and ecology. *Annals of Botany* 126, 4 (03 2020), 539–557.
Y. Zhao and J. Barbič. 2013. Interactive Authoring of Simulation-ready Plants. *ACM Trans. Graph.* 32, 4, Article 84 (2013), 12 pages.

A LIST OF SYMBOLS

T_A	Temperature adaptation (°Celsius)
P_A	Precipitation adaptation (mm)
a_b	Age of a branch segment (years)
d_b	Branch segment diameter (m)
l_b	Branch segment length (m)
M_m	Module biomass (kg)
E_p	Evapotranspiration (mm)
τ	Transpiration coefficient
R	Average precipitation (mm)
q_w	Soil water (mm)
q_o	Surface water (mm)
B	Plant density (kg/m^2)
g_{max}	Maximum water uptake (mm · m^2/ (kg · s))
k_1	Half-saturation constant of water uptake (mm)
α	Maximum infiltration rate (1/s)
β	Scaling coefficient
k_2	Saturation constant of water infiltration (kg/m^2) (kg//m^2)
W_0	Water infiltration rate
r_w	Water loss due to evaporation (1/s)
D_W	Diffusion coefficient for soil water (m^2/s)
D_O	Diffusion coefficient for surface water (m^2/s)
q_v	Water vapor (kg/m^2)
q_c	Condensed water (kg/m^2)
q_r	Rain water from clouds (kg/m^2)
A_C	Autoconversion of rain from clouds (kg/m^2)
K_c	Accretion of cloud water due to falling rain drops (kg/m^2)
E_M	Macroclimatic vapor (kg/m^2)
C_c	Condensation (kg/m^2)
E_r	Evaporation of rain water (kg/m^2)
E	Heat emission (°Celsius)
θ	Heat from ground surface (°Celsius)
P	A plant model
M	Module instance
o	Climatic adaptation parameter
v_r	Maximum vigor value
c	Node in module graph
C_b	Set of all nodes in a module graph
u	A module graph
U	Set of all module graphs in a plant P

B AVERAGE PRECIPITATION GRAPH

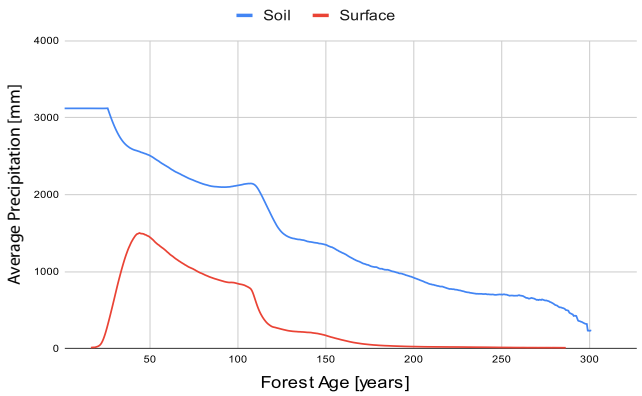

Fig. 25. Plots of average soil and surface water as a function of forest age for simulation results shown in Fig 24. Changing macroscopic vapor E_M results in a decrease of soil and surface water. The shape of graphs indicates the non-linear feedback between vegetation and atmosphere. Our model allows to explore the water dynamics between the vegetation, soil and atmosphere models.

C PERFORMANCE ANALYSIS

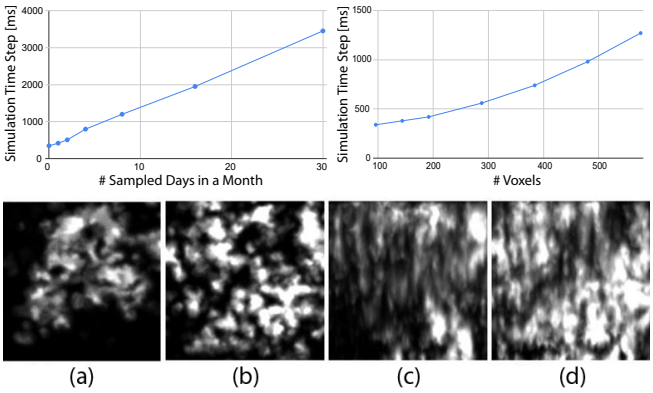

Fig. 26. Top left: computation time of a simulation step (ms) plotted as a function of sampled days for a month in a simulation of 65K plants. One sampled day corresponds to 60 iterations of weather simulation at a time step of 1 minute. This means that we use in this experiment 1 hour of weather simulation to represent a one-day sample. Zero-sampled days describes the case of no weather calculations present in the simulation, meaning just vegetation and soil simulation. The relation of computation time of simulation steps to number of sampled days is approximately linear. Top right: computation time of a simulation step (ms) as a function of voxel number of one bottom side of the WVS for 1-day samples. 196x196 WVS extent over a terrain corresponds to almost 4 km^2 at a resolution of 20m per voxel. The scene corresponding to the rightmost point corresponds to an extent of almost 12 km^2. Bottom: four precipitation maps obtained by sampling 1, 2, 8, and 30 days. while only sampling the weather for one day (a) may result in regions receiving no precipitation, a greater number of sampled days results in smoother, more realistic, precipitation gradients (b-d).

D TABLES

Table 2. Settings and parameter values for figures in the paper. PT=lexigraphical codes of plant types (Table 1), P=Num. Plants at simulation end (k), M=Num. Modules (k), T=Total time of simulation (years), TS=Computation time of one Simulation Year (s), EVS=Ecosystem Voxel Space, WVS=Weather Voxel Space, $D_W = 0.01$, $D_O = 10$, WVS size is matching EVS size in x-z extent and 1000 cells in y-direction.

Fig.	PT	P	M	T	TS	EVS	WVS	E	E_M	f_w
1	cdij	200	1000	250	8.0	400	20	1.5	0.2	0.6
11	g	50	100	0.1	0.8	400	20	2.4	0.25	0.0
12	h	140	200	300	2.6	400	20	2.1	0.5	0.2
14a	a	30	60	0.1	0.6	1200	20	1.5	0.2	0.1
14b	j	20	50	0.1	0.7	1200	20	1.5	0.2	0.1
14c	h	180	400	0.1	2.9	1200	20	1.5	0.2	0.1
14d	h	90	200	0.1	1.6	1200	20	1.5	0.2	0.1
15	ab	61	88	100	0.6	400	40	1.5	0.25	0.1
16	defklm	150	700	300	4.5	400	20	2.7	0.59	0.1
17	abg	23	71	100	0.5	200	20	2.4	0.25	0.0
18	cdij	200	1000	250	8.0	1000	20	1.5	0.2	0.6
23	ag	50	100	150	0.8	400	20	2.4	0.25	0.0
24	defklm	300	603	200	7.0	400	20	2.4	0.02 - 0.25	0.1

Table 1. Parameter values of plant types used to generate the results shown in this work. Please see [Makowski et al. 2019] for a description of all parameters.

Tree	Seed. Freq.	Seed. Rad.	s_{tol}	T_A	P_A	p_{max}	$\bar{v}_r$	g_p	λ/λ_m	D/D_m	F_{age}	α	ω_2	g_1	ϕ	β	τ
(a) Shrub I	2.5	3.2	0.61	7.5	1068	9	67	1.5	0.37	0.16	1	0.18	0.15	0.06	4.4	2.4	0.08
(b) Shrub II	2.6	5.3	0.1	29.5	682	6	22	0.93	0.45	0.45	1	0.16	0.81	0.09	1.2	1.9	0.08
(c) Shrub III	1.0	10	0.1	8.1	682	30	2	0.7	0.38	0.39	5	0.49	0.49	2.5	2.3	3.5	0.08
(d) Shrub IV	1.0	7	0.48	6.3	453	42	5	0.186	0.64	0.64	5	0.52	0.63	0.9	3	2.7	0.08
Shrub V	1.0	60	0.52	27	2592	95	10	0.45	0.48	0.87	10	-0.3	0.76	0.19	2	2.5	1.0
(e) Shrub VI	1.0	60	0.28	28	2592	68	5	0.56	0.64	0.64	5	0.52	0.63	0.9	1.8	1.5	1.0
(f) Shrub VII	1.3	60	0.24	27	1883	40	3	0.5	0.56	0.3	3	0.35	0.57	0.9	1.5	1.1	1.0
(g) Conifer I	2.7	1.8	0.66	8.1	1154	120	54	0.35	0.79	0.86	12	-0.19	0.81	3.5	3	5.2	0.08
(h) Conifer II	0.7	2.1	0.52	10.0	853	220	60	0.28	0.79	0.86	12	-0.19	0.81	3.5	1.5	5.2	0.08
(i) Conifer III	1.0	1.5	0.3	9.26	512	120	135	0.53	0.79	0.86	12	-0.19	0.81	0.17	1.9	2.4	0.08
(j) Deciduous I	1.5	2.6	0.55	11.5	840	135	225	0.8	1/0.46	0.8/0.3	20	-0.45	0.58	1.9	4.1	2.4	0.16
(k) Deciduous II	1.0	50	0.58	27	2966	130	140	0.48	0.9/0.62	0.87/0.25	20	0.52	0.63	0.69	2.3	1.7	1.0
(l) Palm	3.8	2.9	0.39	27	3100	73	67	1.5	1	1	10	0.69	0.88	2.1	3.7	13	1.0
(m) Cocoa	1.0	10	0.62	27	2835	180	230	0.62	0.7	0.67	15	-0.56	0.5	1.3	1.3	2.6	0.5